Received: 11 August 2022 | Revised: 11 February 2023 | Accepted: 21 February 2023

DOI: 10.1002/suco.202200743

ARTICLE

fib CEB-FIP WILEY

Experimental investigation on the use of Fabric-Reinforced Cementitious Mortars for the retrofitting of reinforced concrete dapped-end beams

Katherina Flores Ferreira | **Marco Carlo Rampini** | **Giulio Zani** | **Matteo Colombo** | **Marco di Prisco**

Department of Civil and Environmental Engineering, Politecnico di Milano, Milan, Italy

Correspondence
Katherina Flores Ferreira, Department of Civil and Environmental Engineering, Politecnico di Milano, Piazza Leonardo da Vinci, 32 - 20133 Milano, Italy.
Email: katherina.flores@polimi.it

Funding information
CSLLPP RELUIS Agreement DM 578/2020; RELUIS WP14 - 2019/2021

Abstract

The structural performance and durability of reinforced concrete (RC) dapped-end beams may be significantly threated by the effects of deterioration and environmental actions, compromising the structural robustness of important infrastructures such as bridges. The study of the critical role of dapped-ends has grown in recent years, focusing in particular on the implementation of innovative retrofit solutions capable of extending the service life of these structural elements. In this paper, an experimental investigation on the contribution of Fabric-Reinforced Cementitious Matrix (FRCM) retrofitting system to the load bearing capacity of RC dapped-end beams is presented. A set of eight full-scale dapped-ends was subjected to monotonic loading tests. The presence of cracks prior to the application of the retrofitting composite, which may represent the actual state of conservation of existing RC half-joints subjected to heavy traffic loads, is reproduced by testing the specimens up to the reaching of the ultimate design load. Different orientations of the alkali-resistant glass fabric composing the FRCM system were tested, and the results allow to discuss the effectiveness of the retrofitting solution.

KEYWORDS

AR-glass fabric, crack patterns, dapped-end beam, fabric-reinforced cementitious mortar, FRCM retrofitting, load bearing capacity, RC half-joint

1 | INTRODUCTION

Reinforced concrete (RC) dapped-end beams are structural elements in which the depth of the extreme section is significantly reduced and extended up to a certain portion of the beam, creating a so-called nib. The study of the shear behavior of RC dapped-end beams dates back to the early 1950s,[1,2] when its use started to

Discussion on this paper must be submitted within two months of the print publication. The discussion will then be published in print, along with the authors' closure, if any, approximately nine months after the print publication.

spread in the field of precast constructions as half-joints between two precast members (e.g., half-joint beam of RC bridge). The application of simplified strut-and-tie models for the design of RC dapped-ends has been widely validated in the last decades,[3,4] with particular attention to the optimal dimensions of the dapped-end and the evaluation of the effects of the reinforcement layout in the load bearing capacity of the beams.[5–8] Despite the design and construction simplifications associated to these elements, they represent a critical structural component due to their usually reduced possibility of inspection, and their exposure to environmental actions, especially in case of bridge infrastructures. Recent events involving the collapse of bridges with RC half-joints highlighted the influence of this type of element on the structural robustness, especially when not properly designed or built in accordance to the bridge class required.[9] Furthermore, the propagation of shear cracks may facilitate the oxidation of the steel reinforcement, leading to the failure of the element even when subjected to ordinary live loads.[10]

In Italy, the use of cement-based composites for retrofitting interventions of existing infrastructures has widely spread during the last years, after the promulgation of national regulations that describe the procedure for the identification, the use, and the characterization of this type of retrofitting technique.[11,12] Multiple studies[13–17] have been conducted over the last two decades to investigate the contribution of cement-based composites to the structural behavior of new and existing masonry and concrete structures. This solution can significantly improve the durability, the flexural capacity, and the shear strength of reinforced-concrete members. However, few data on the application of composite materials for the retrofitting of critical high-bearing details such as dapped-end joints is present in the literature. These works are mainly focused on the use of Carbon Fiber-Reinforced Polymers,[18–20] with no evidence on the use of Fabric-Reinforced Cementitious Matrix (FRCM) as retrofitting solution for dapped-end beams. Externally bonded reinforcements are particularly suitable for the retrofitting of discrete dapped-ends and in the absence of transverse beams in close proximity to the nib. This paper presents an experimental investigation on the use of FRCM for the retrofitting of RC dapped-end beams. The load bearing capacity and the overall structural behavior of retrofitted specimens are evaluated and compared with respect to reference unretrofitted beams. A total number of eight dapped-end joints was tested. Six of these samples were retrofitted with a specific FRCM system, after being loaded up to the design ultimate load. This induced a crack pattern typically encountered in an infrastructure that reached the ultimate limit state (ULS) design load at least one time over its service life. Two unretrofitted samples were tested up to failure to provide the reference response of the structural element. Then, three different FRCM retrofitting systems were experimentally investigated considering the variation in fabric orientation and number of layers. Two nominally identical specimens were tested for each retrofitting solution.

The experimental campaign was carried out in the framework of the RELUIS WP14 – 2019/2021 project for the evaluation of the effects of using innovative materials as retrofitting solutions. The structural behavior of the unretrofitted specimens was taken as reference for the validation of existing design approaches implemented in the framework of the WP4-T4.4 (Gerber Saddles) CSLLPP RELUIS Agreement DM 578/2020.

TABLE 1 Concrete mix design.

Mix design	(kg/m^3)
Cement CEM I 52.5R	280
Aggregate 1 (0–3 mm)	620
Aggregate 2 (0–12 mm)	440
Aggregate 3 (8–15 mm)	710
Water	175
Limestone filler	120
Superplasticiser	5.5

2 | MATERIALS

The materials used both for the production of the RC dapped-end samples and for the retrofitting with fabric-reinforced cementitious composites are discussed in this section.

2.1 | Concrete

Dapped-end specimens were cast in two different batches adopting the same concrete mix design shown in Table 1, characterized by a water-to-cement ratio equal to 0.63. A total number of 18 nominally identical cubic specimens (nominally 100 mm side) was cast to proceed with the mechanical characterization of the material (6 specimens from the first batch and 12 from the second one). The characterization consisted in 12 uniaxial compressive tests performed on cubic samples and tensile splitting tests carried out on twelve $100 \times 100 \times 50$ mm^3 specimens (obtained cutting six cubes in half). In order to obtain an estimation of the mechanical properties at the different phases of the experimental campaign, half of the concrete specimens were tested in parallel with the reference and pre-damaged dapped-ends tests (after 35–53 days of natural curing), while the remaining samples were tested together with the retrofitted dapped-ends (at around 220 days of natural curing).

TABLE 2 Concrete compressive strengths of specimens: discrete values, average values, and coefficient of variation.

Batch no.	Specimen	Curing days	f_{cc} (MPa)	$f_{cc,av}$ (MPa)	COV (%)
1	N01	38	60.99	58.58	5.83
	N02	38	56.16		
	N03	223	59.20	57.18	5.00
	N04	223	55.16		
	Average	–	–	57.88	4.03
2	N05	35	45.49	45.70	1.70
	N06	35	44.82		
	N07	35	46.69		
	N08	35	45.79		
	N09	220	48.40	46.86	3.64
	N10	220	44.82		
	N11	220	48.12		
	N12	220	46.09		
	Average	–	–	46.28	2.78

TABLE 3 Concrete splitting tensile strengths of specimens: discrete values, average values, and coefficient of variation.

Batch no.	Specimen	Curing days	$f_{ct,sp}$ (MPa)	$f_{ct,sp,av}$ (MPa)	COV (%)
1	N01	53	3.78	3.73	1.81
	N02	53	3.68		
	N03	222	3.35	3.65	11.82
	N04	222	3.94		
	Average	–	–	3.69	5.82
2	N05	50	2.95	3.02	4.74
	N06	50	2.85		
	N07	50	3.13		
	N08	50	3.15		
	N09	219	3.15	2.92	5.80
	N10	219	2.75		
	N11	219	2.84		
	N12	219	2.95		
	Average	–	–	2.97	4.87

The results of the uniaxial compressive and splitting tensile tests are reported in Table 2 and Table 3. Relevant strength differences were noticed among specimens coming from the two batches. In particular, specimens from the first one presented an average cubic compressive strength ($f_{cc,av}$) of 57.88 MPa (Table 2), and an average splitting tensile strength ($f_{ct,sp,av}$) of 3.69 MPa (Table 3), while specimens from the second batch showed lower strength values, with a $f_{cc,av}$ equal to 46.28 MPa (Table 2) and $f_{ct,sp,av}$ equal to 2.97 MPa (Table 3). On the contrary, negligible discrepancies were encountered concerning the influence of testing age. Please note that to obtain the tensile strength of the material (f_{ct}), a coefficient between the uniaxial and the splitting tensile strengths equal to 1 may be used ($f_{ct} = f_{ct,sp}$), according to MC2010.[21]

2.2 | Steel

The steel reinforcement used in the samples was made of ribbed bars with a nominal yield strength of 450 MPa and a ductility grade C (B450C). Different bar diameters were considered, in accordance with the reinforcement layout described in Section 3.2. The results of the uniaxial tensile tests are reported in Table 4 in terms of average yield strength ($f_{y,av}$), average tensile strength ($f_{t,av}$), and average strain at maximum tensile force ($A_{gt,av}$, measured according to the procedure established in ISO 6892-1[22]) for each rebar diameter used. As an example, the tensile stress–strain curves obtained from tests on Φ12 mm bars are depicted in Figure 1.

Rebar diameter (mm)	No. of tests	$f_{y,av}$ (MPa)	$f_{t,av}$ (MPa)	$A_{gt,av}$ (%)
10	6	526.5	623.7	8
12	6	530.2	628.2	13
14	6	507.7	627.5	10
20	3	555.0	677.7	11
26	3	522.7	634.7	12

TABLE 4 Average mechanical properties of steel rebar.

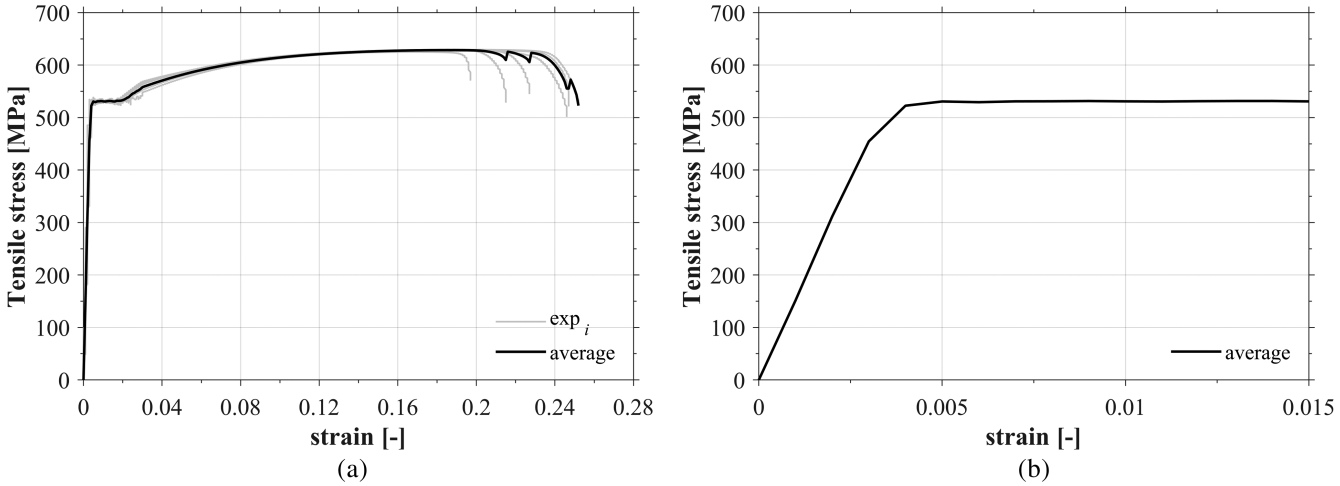

FIGURE 1 Uniaxial tensile stress–strain curves of 12 mm diameter bars (a), and detail of the average curve in the 0–0.015 strain range (b).

2.3 | FRCM composites and mortar-to-substrate interface properties

In this section, the geometrical and mechanical properties of the FRCM system used for the retrofitting of the pre-damaged dapped-end beams are described. The system was composed of an alkali-resistant (AR) glass fabric and a commercial shrinkage-compensated thixotropic cement-based mortar, particularly suitable for repair applications on concrete members. The mechanical characterization of both the fabric samples (70×400 mm^2 size) and the cement-based mortar is taken from the experimental results already documented in the literature by the authors.[23] It is important to highlight that the dimensions and test procedures adopted for the characterization of the FRCM composites (Section 2.3.2) and the mortar-to-substrate interface (Section 2.3.3) were different from those established in the National Italian Guidelines.[12] This choice was done in order to compare the parameters related to the efficiency of the reinforcement with those obtained in the reference FRCM characterization campaign,[23] which was carried out prior to the publication of the Italian Guidelines.[11,12]

2.3.1 | AR glass fabric and cementitious repair mortar

The selected AR-glass fabric was a double leno weave mesh, impregnated with an epoxy resin, and woven with a symmetric glass content along the two perpendicular directions (warp and weft). The main geometrical and mechanical tensile properties of the fabric are summarized in Table 5. The average peak load ($P_{max,av}$) was obtained from five nominally identical uniaxial tensile tests performed on each direction of the reinforcement. The fabric efficiency factor (EF_f) indicates the rate of utilization of the fabric. It is a function of the average peak load, of the equivalent cross-sectional area embedded (A_f), and of the glass filament strength, assumed equal to 2000 MPa as declared by the manufacturer.[24]

The mix design of the commercial cement-based shrinkage-compensated thixotropic mortar is displayed in Table 6. The mechanical characterization of the matrix carried out from Rampini et al.[23] consisted in bending and compressive tests performed on six nominally identical prismatic specimens, from which an average flexural tensile strength f_{ctf} of 7.02 MPa (std 1.32 MPa) and a

TABLE 5 AR-glass fabric characteristics.

Characteristics	Warp	Weft
Fabrication technique	Double leno weave	
Coating nature	Epoxy	
Wire spacing (mm)	38	38
Roving fineness (Tex)	4 × 2400[a]	4 × 2400
Filament diameter (μm)	27	27
Equivalent reinforcement thickness (mm)	0.093	0.093
Average tensile peak load, $P_{max,av}$ (kN/m)	162.50[b]	152.10
Fabric efficiency factor, EF_f	0.87	0.82

Abbreviation: AR, alkali-resistant.

[a]This value corresponds to the global weight aligned in the warp direction.

[b]Average of only four tests. One of the test was discarded due to clamping misalignment.

cubic compressive strength f_{cc} of 58.94 MPa (std 7.35 MPa) were obtained.

2.3.2 | FRCM composites

In parallel with the application on the RC dapped-ends, in order to investigate the mechanical performance of the system by means of uniaxial tensile tests, three nominally identical FRCM coupons (70 × 400 × 9 mm^3 in size) were cast, both with the warp and the weft parallel to the long side of the sample (400 mm). Specimens were clamped at the testing machine imposing a clamping force of about 12 kN and steel plates (70 × 50 × 1 mm^3) were glued at the ends of the specimens to prevent stress localization within the clamping regions. A nominal free length (L_0) of 300 mm was chosen, consistently with the tensile tests conducted on fabric specimens. To measure the integral crack opening displacements (CODs) astride a gauge length (GL) of 200 mm, two linear variable differential transformers (LVDTs) were placed on the two sides of the sample. The tests were displacement-controlled imposing a constant cross-head displacement (stroke, δ) rate of 0.02 mm/s by means of an electro-mechanical machine with a maximum load capacity of 30 kN. It is worth mentioning that this rate differs from the one suggested by the Italian Guidelines[12] (0.0033 mm/s) and possible effects of the strain rate on the mechanical performances of the composites[25,26] would merit proper verification before application on real structures.

The results of the uniaxial tensile test are reported in Figure 2 in terms of nominal stress on the cross-section of the specimen (σ_{FRCM}) versus normalized displacement (δ/L_0) for both the warp and the weft reinforcement direction. From the curves, it is possible to identify the typical behavior of FRCM composites, which consists of a first linear-elastic branch, followed by a multi-cracking phase and a third region dominated by the fabric response. Relevant geometrical and mechanical quantities related to the uniaxial characterization of the FRCM system are collected in Table 7. In particular, the composite efficiency (EF_{FRCM}) corresponds to the ratio between the average maximum loads recorded in the composite and those of the fabric tensile tests.[23] In Figure 3, the comparison between the fabric and the composite tensile responses is reported. For the FRCM strips, the strain values (ε) are obtained starting from the COD measurements ($\varepsilon = COD/L_G$). Please note that curves in which COD measurements were lost are not depicted in the graphs.

TABLE 6 Cement-based matrix mix design.

Mix design	(kg/m^3)
R4 (EN 1504-3:2005)[13] shrinkage-compensated, thixotropic premixed mortar	1840
Water	276
Curing agent specifically indicated for the premixed mortar	18.4

2.3.3 | Mortar-to-substrate interface

Two single-lap shear tests were carried out to investigate the bond-slip behavior at the interface between the FRCM composite and the concrete substrate. Test specimens consisted of a FRCM reinforcement strip (70 × 150 × 12 mm^3 in nominal size) applied on concrete blocks cast with the same concrete of the dapped-ends. The substrates were subjected to a hydro-scarification with a pressure of around 1000–1200 atm (the same used to prepare the concrete substrate of the dapped-ends), in order to increase bond and guarantee the full exploitation of the FRCM reinforcing capacity.[27] A limited bond length of 150 mm was set to promote the detachment of the reinforcement from the support and to highlight the effect of substrate roughness. This value was lower than the effective anchorage length of around 200–300 mm, as documented in literature.[28] Only the warp direction of the fabric was considered, due to its higher performance. The tests were displacement-controlled at a machine crosshead displacement (stroke, δ) rate of 0.01 mm/s (also in this case, possible effects of the strain rate should be checked) and the experimental set-up is illustrated in Figure 5a. Two LVDT transducers ($\delta_{top,left/right}$) were arranged in order to measure the relative displacement of the head of the reinforcement strip (outer surface) with respect to the concrete substrate. An additional LVDT transducer was placed at

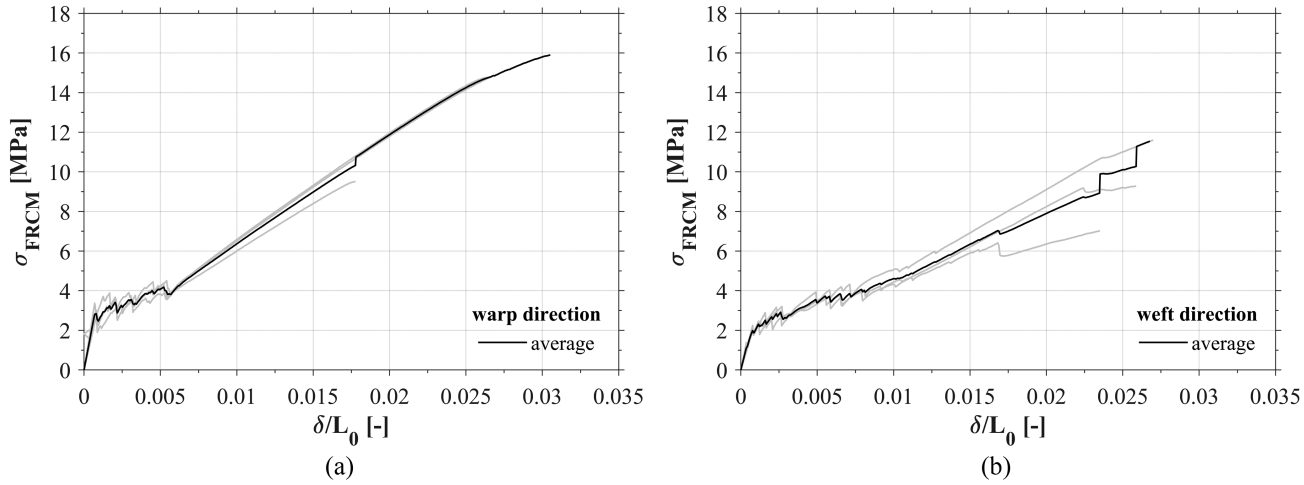

FIGURE 2 Tensile response of the FRCM system in terms of nominal stress σ_{FRCM} versus normalized displacement δ/L_0: in the warp (a) and weft directions (b). FRCM, Fabric-Reinforced Cementitious Matrix.

TABLE 7 Relevant geometrical and mechanical parameters of FRCM composites under uniaxial tension: average values (avg.) and standard deviations (std).

		Thickness (mm)	Width (mm)	L_0 (mm)	$P_{FRCM,max}$ (kN)	$P_{fabric,max}$ (kN)	EF_{FRCM} (−)
Warp direction	avg.	9.69	70.56	289.33	9.08	12.50	0.73
	(std)	(0.57)	(0.31)	(2.08)	(1.98)	(6.68)	(−)
Weft direction	avg.	10.94	70.79	288.33	7.15	11.70	0.61
	(std)	(0.53)	(0.75)	(1.53)	(1.45)	(7.52)	(−)

Abbreviation: FRCM, Fabric-Reinforced Cementitious Matrix.

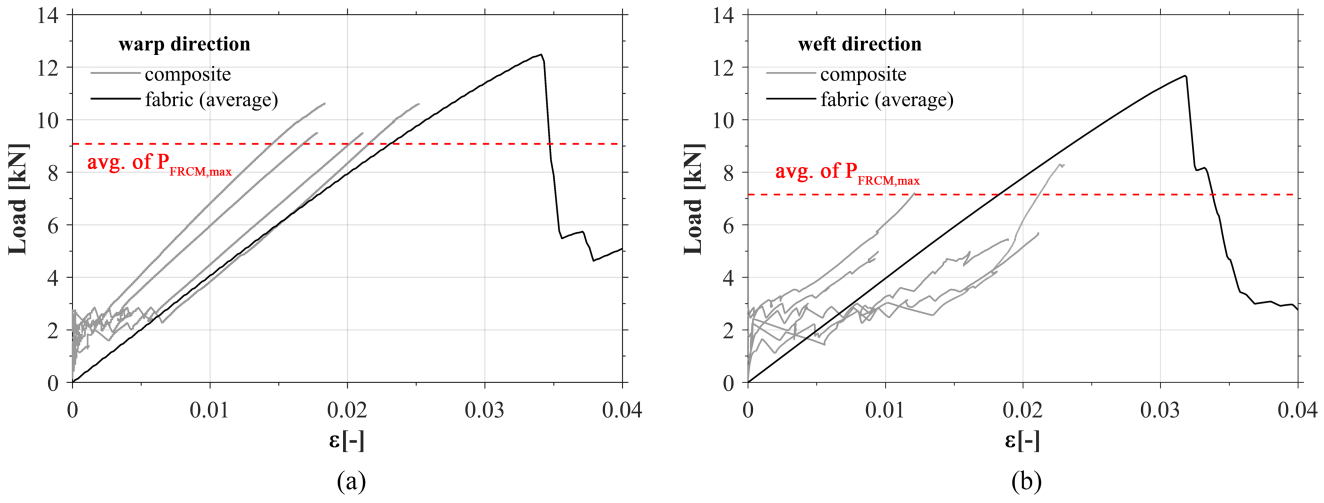

FIGURE 3 Comparison between the composite and the fabric tensile responses considering the same width of the samples (70 mm): load versus ε curves in (a) warp and (b) weft directions. Red dashed lines represent the average maximum tensile load of the composite.

the middle of the strip to monitor any formation of cracks on the outer FRCM surface. The failure mode in both tests was governed by the rupture of the fabric not embedded in the matrix (Figure 5b,c) and the maximum loads (P_{max}) reached were equal to 10.44 kN and 10.38 kN, respectively for the first and the second test. They resulted higher than the average capacity of the FRCM under tensile actions (Table 7). This confirms the suitability of the substrate roughness to fully exploit the overall composite reinforcing action, if bonded to the support for at least 150 mm from

the FRCM cross-section subjected to a stretching action. However, this conclusion is closely related to the composite under study and therefore it should not be generalized to all FRCM composites. In fact, previous studies on the bond behavior of different FRCM composites[29] have shown lower tensile strengths than those obtained from the corresponding tensile tests.

The results of the single-lap shear tests are plotted in Figure 4 in terms of load (P) versus stroke (δ) and load (P) versus top mortar displacement (δ_{top}), being the latter calculated as the average between $\delta_{top,left}$ and $\delta_{top,right}$. Please note that, in the first test (black lines in Figure 4a), the increase of the top mortar displacement measure was related to a partial ejection of the external mortar layer and the consequent loss of the instrument reference (as visible in Figure 5b, the failure was related to the fabric rupture). No clear information can be provided on the slippage of the fabric within the mortar due to the absence of adequate instruments to measure this phenomenon. It is possible to assume that the slip occurred only after around 7 kN, as visible from Figure 4b in which the single-lap shear responses in terms of load (P) versus stroke (δ) are compared with the fabric response in tension (obtained normalizing the curve in Figure 3a with respect to the nominal free length of the fabric in the shear tests). The actual fabric slippage could be investigated in future studies, following the test procedure suggested by the Italian Guidelines.[12]

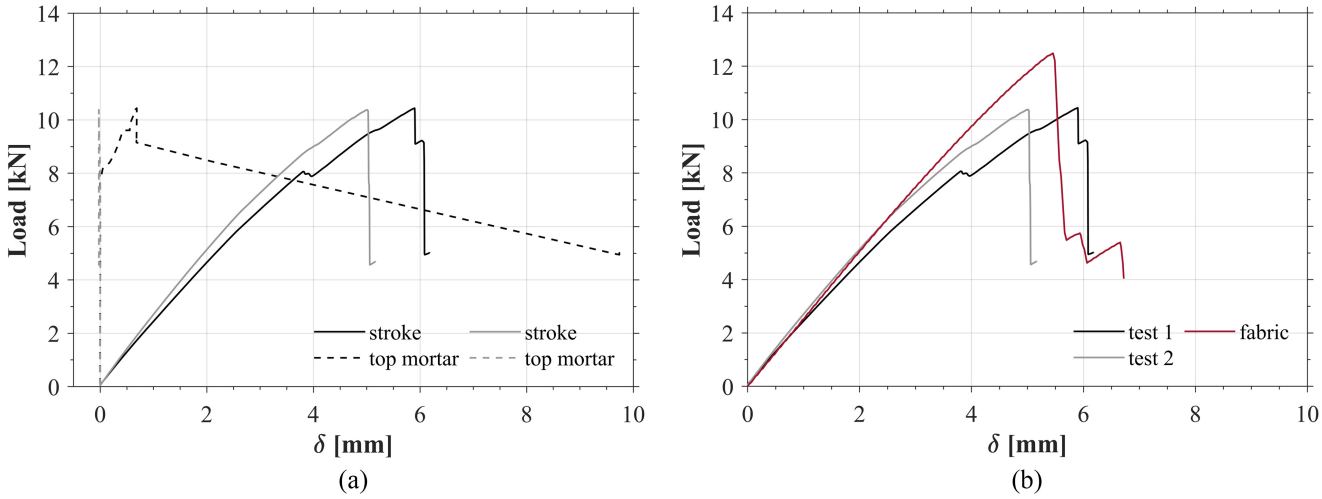

FIGURE 4 Single-lap shear tests: Load-stroke and Load-top mortar displacement (δ_{top}) curves (a), and comparison between Load-stroke curves and the fabric (warp direction) tensile response (b).

FIGURE 5 Single-lap shear tests: test set-up and instrumentation (a), failure mode of the first (b), and the second specimen (c).

TABLE 8 Summary of the experimental program on RC dapped-end beams.

Specimen ID	Test procedure	Number of fabric layers	Fabrics orientation
REF-01	Failure test	–	–
REF-02			
PRE-01 to 06	Pre-damage test up to 270 kN	–	–
RTF-(0°)-01	PRE-02 + retrofitting + failure test	1	0°
RTF-(0°)-02	PRE-01 + retrofitting + failure test		
RTF-(45°)-01	PRE-04 + retrofitting + failure test	1	45°
RTF-(45°)-02	PRE-03 + retrofitting + failure test		
RTF-(0° + 45°)-01	PRE-06 + retrofitting + failure test	2	1 layer at 0° 1 layer at 45°
RTF-(0° + 45°)-02	PRE-05 + retrofitting + failure test		

Abbreviation: RC, reinforced concrete.

3 | EXPERIMENTAL CAMPAIGN DESCRIPTION

3.1 | Experimental program

Eight full-scale RC dapped-ends were tested. Two were tested up to failure, to determine the reference load bearing capacity (P_{max}) of the specimens. The remaining six elements were used to analyze the influence of the FRCM retrofitting solution on the load bearing capacity of pre-damaged specimens. Thus, these dapped-ends were initially loaded up to the reaching of the analytically estimated ultimate design load, $P_{PRE} = P_{Rd}$, equal to 270 kN (see Section 4.2). After the pre-damaging phase, the beams were retrofitted with the FRCM composite previously presented (see Figure 10) and tested up to failure. In the retrofitting applications, the variability of the fabric orientation (0° or 45° degrees between the horizontal direction and the warp wires), and the number of layers constituting the composite (one or two layers) were considered. All the details regarding the experimental program are summarized in Table 8. Note that the tests are identified using the following notation: an acronym that specifies the type of specimen (REF = reference; PRE = pre-damaged or RTF = retrofitted), the orientation of the warp with respect to the horizontal direction for retrofitted specimens (0°, 45°, or 0° + 45° to indicate two crossed layers), and a number indicating the repeatability of nominally identical tests (01 or 02).

3.2 | Geometry of specimens, test set-up, and instrumentation

The geometry of the samples and test set-up is illustrated in Figure 6a. Each beam element had two dapped-ends, which were individually tested. The overall length of the four beam specimens was 3500 mm, with a rectangular full-depth cross-section of 250 × 650 mm^2. The length of the nib was 300 mm, while its depth was set equal to 325 mm (half of the full-depth of the beam). Two beams, corresponding to REF-01/02 and PRE-01/02 dapped-ends, were realized with concrete from the first batch, while the other two elements came from the second cast. All beam specimens were cast adopting the same steel reinforcement layout, with a minimum effective concrete cover of 20 mm (Figure 7). The adopted layout was established according to previous experimental studies reported in the literature.[7] In particular, the dapped-end reinforcement comprised two layers of Φ14 diagonal rebars and three layers of Φ12 U-shaped horizontal rebars. Top and bottom flexural reinforcements were oversized and provided along the full length of the beam, in order to prevent the flexural failure far from the tested joint. Shear reinforcement comprised Φ10 vertical stirrups placed at variable distances (from 100 mm to 150 mm, respectively near and far from the dapped-ends).

In order to test each dapped-end reversing the beams after the first test, all specimens were subjected to three-point nonsymmetric bending, under simply-supported conditions (total span equal to 3000 mm). The vertical load was applied at 1000 mm (one-third of the span length) from the tested support by an electromechanical actuator with maximum load capacity of 1000 kN. Supports were composed of a welded 50 mm diameter steel cylinder bearing the dapped-end, and a 250 × 100 × 20 mm^3 steel plate supporting the full-depth section of the beam at the other side. A rubber pad (100 × 250 × 10 mm^3) was placed between the loading device and the specimen to uniformly distribute the load, preventing stress concentrations. The same was done at the two supports by using 2 mm thick rubber sheets. The loading device adopted for the test REF-01 is shown in Figure 8a. Note that this was slightly changed for the remaining tests (Figure 8b), to avoid possible

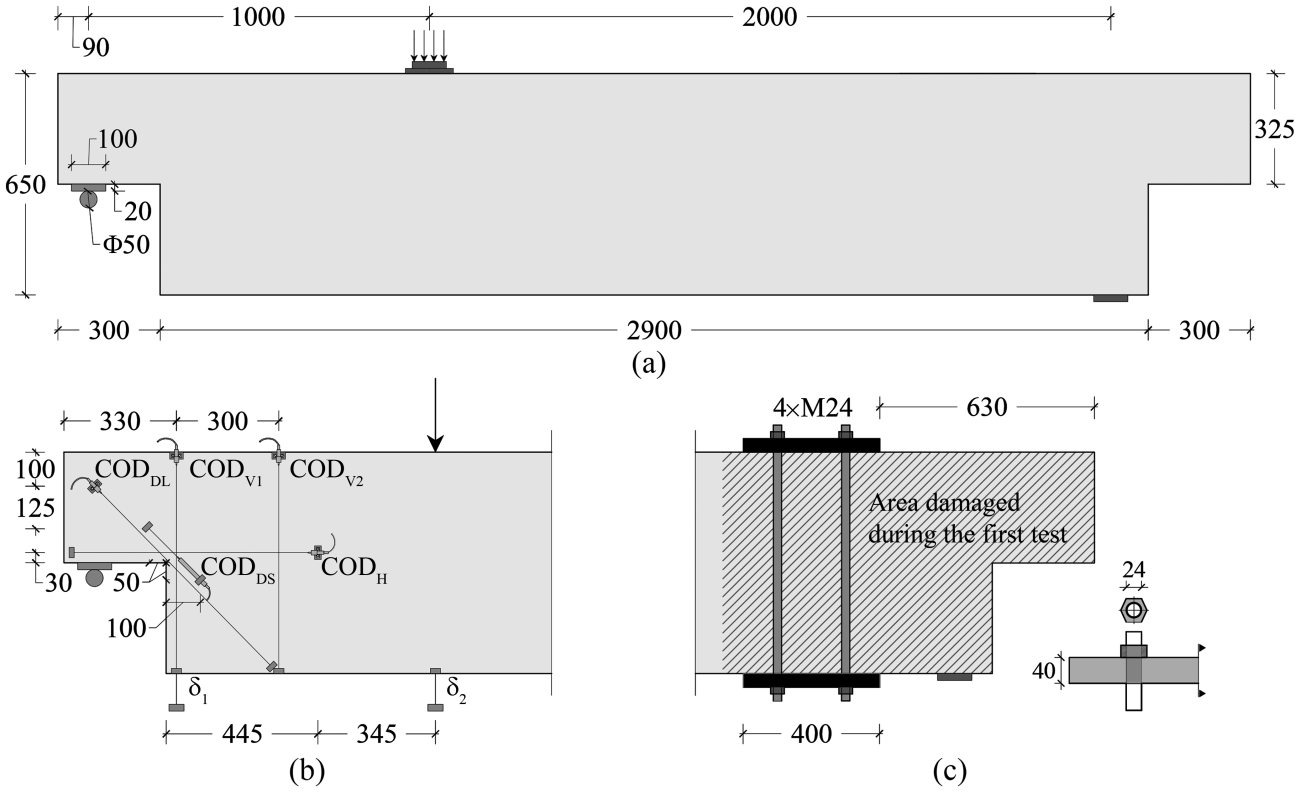

FIGURE 6 Geometry of specimens and test set-up (a), instruments layout (b), and detail of vertical reinforcing plates used after testing the first dapped-end (c). Measures in mm.

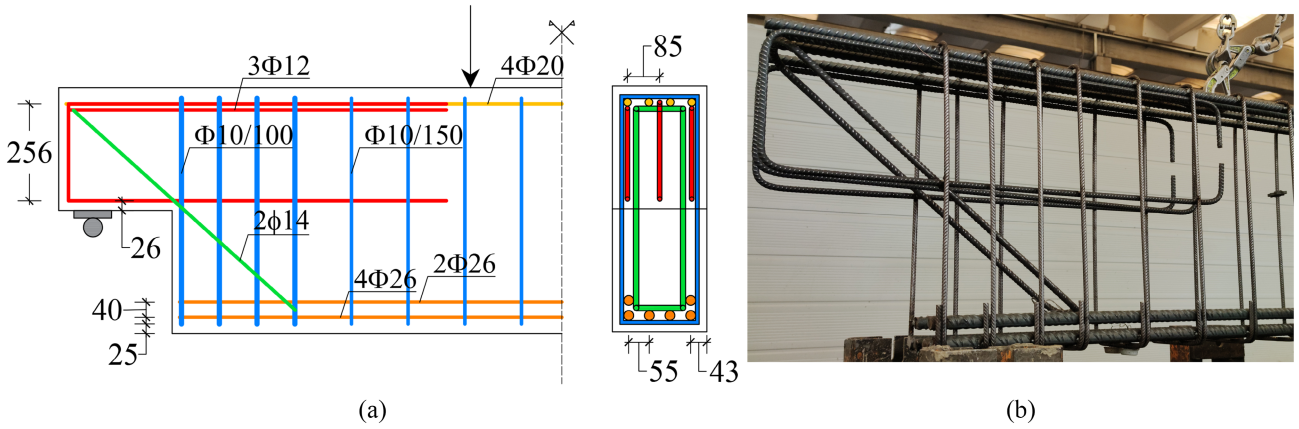

FIGURE 7 Steel reinforcement layout of beam specimens (a) and picture of the cage (b). Measures in mm.

confinement effects due to anomalous mechanical behavior of the support (Figure 8c). Two load cells (maximum load capacity of 200 kN each) were located underneath the steel cylinder support to measure the vertical reaction on the tested dapped-end and to check whether the measured reaction corresponded to the two-thirds of the total applied load, according to the static configuration.

The tests were displacement-controlled at a constant stroke rate of 20 μm/s and carried out according to the following sequence for each beam: (i) testing of the first dapped-end; (ii) unloading; (iii) reversing of the beam and vertical post-compressing of the already tested side of the beam by means of steel plates vertically connected with external post-tensioned steel bars (Figure 6c); (iv) testing of

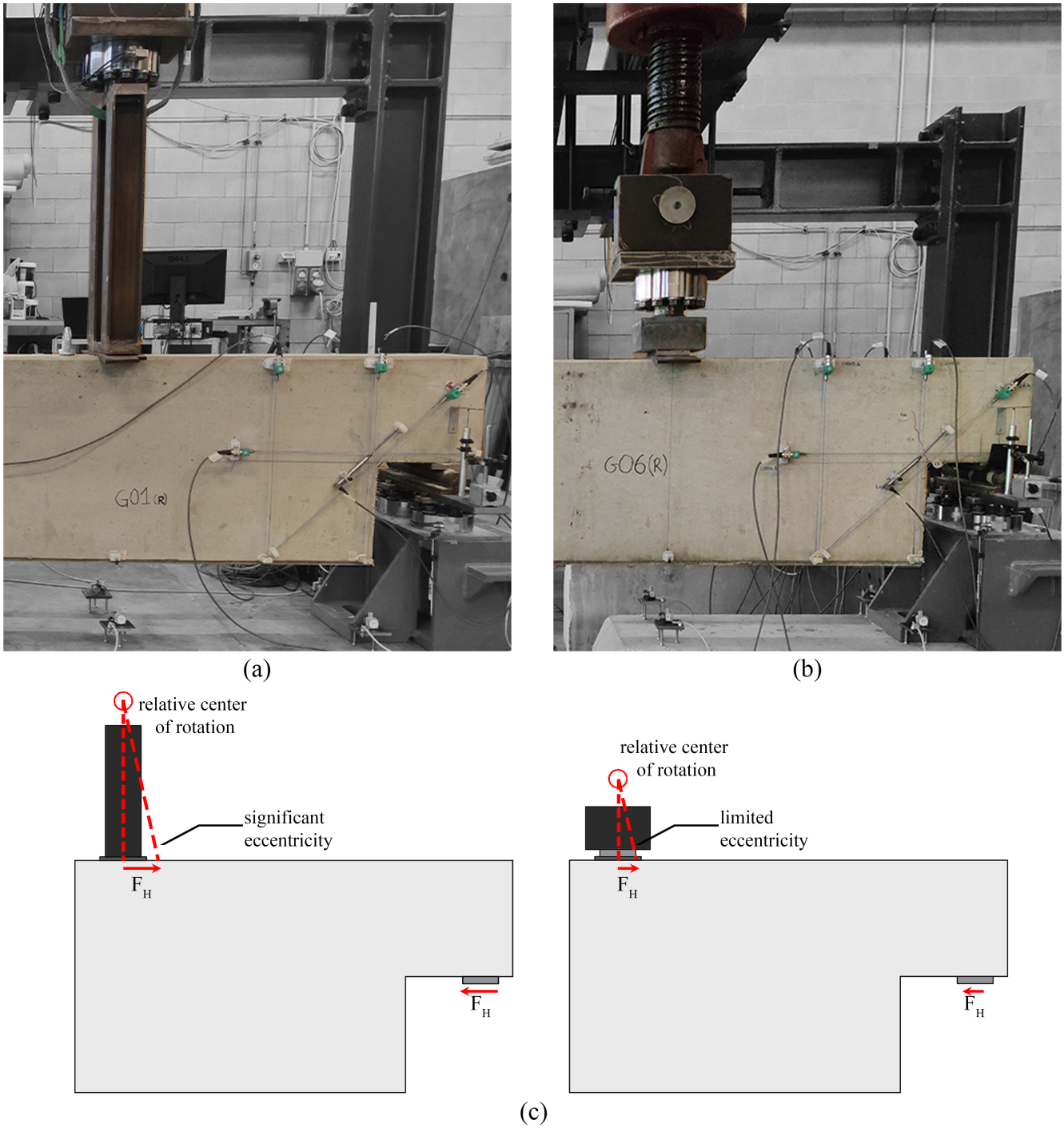

FIGURE 8 Details of the loading device adopted for: specimen REF-01 (a), others (b), and schematic representation of their mechanical behavior (c).

the second dapped-end; and (v) unloading. The structural response of the dapped-end (both in the pre-damage and the failure tests) was monitored arranging the instruments on both the front and back sides, in correspondence to the main rebar layout (Figure 6b). To measure the COD in the diagonal, horizontal, and vertical directions, each side was instrumented with four potentiometric displacement transducers, PDTs (COD_{DL}, COD_{V1}, COD_{V2}, COD_{H}) and one LVDT (COD_{DS}). Moreover, two wire deformometers per side were fixed to the ground to measure the vertical displacements (δ_1, δ_2). It is worth mentioning that both the PDTs and the LVDTs were characterized by a nominal measuring range of 10 mm. Data acquisition was performed at a rate of 1 Hz by an electronic measurement system.

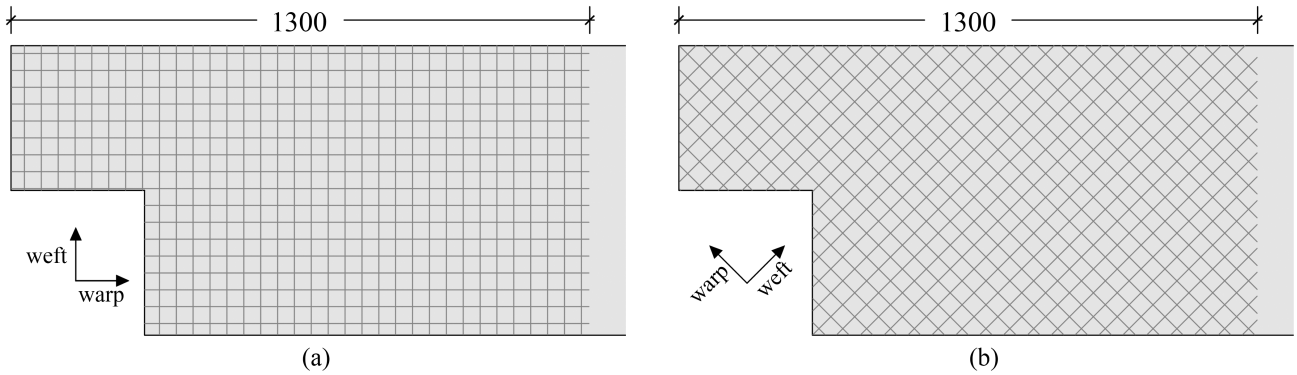

FIGURE 9 Fabric orientation of the FRCM retrofitting systems: layer at 0° (a) and at 45° (b). Measures in mm. FRCM, Fabric-Reinforced Cementitious Matrix.

FIGURE 10 Application of the FRCM retrofitting system on the RC dapped-end beam: hydro-scarification of RC beam surface (a), placing of the fabric layer at 0° (b), placing of the fabric layer at 45° (c), and cast of the finishing layer (d). FRCM, Fabric-Reinforced Cementitious Matrix; RC, reinforced concrete.

TABLE 9 Effective thickness of the applied FRCM retrofitting layers.

Specimen	Specimen side	Thickness (mm) measured on drilled cylinder no.				
		1	2	3	4	Average
RTF-(0°)-01	Front	18.84	18.56	19.98	–	19.13
	Back	21.82	20.38	16.66	–	19.62
	Total	285	285	287	–	286
RTF-(0°)-02	Front	19.97	19.91	18.25	20.55	19.67
	Back	20.32	18.91	22.30	18.55	20.02
	Total	282	280	284	283	282
RTF-(45°)-01	Front	18.26	18.57	18.88	–	18.57
	Back	18.51	25.43	18.96	–	20.97
	Total	283	282	285	–	283
RTF-(45°)-02	Front	22.17	17.35	15.64	18.08	18.31
	Back	21.60	21.07	20.98	18.17	20.46
	Total	284	283	283	283	283
RTF-(0° + 45°)-01	Front	18.03	23.94	21.63	–	21.20
	Back	21.28	20.83	18.40	–	20.17
	Total	280	284	280	–	281
RTF-(0° + 45°)-02	Front	18.16	19.63	18.42	–	18.74
	Back	19.67	20.18	19.03	–	19.63
	Total	279	280	280	–	280

Note: Values measured from Φ8 mm drilled cylinders: FRCM layers and total thicknesses.
Abbreviation: FRCM, Fabric-Reinforced Cementitious Matrix.

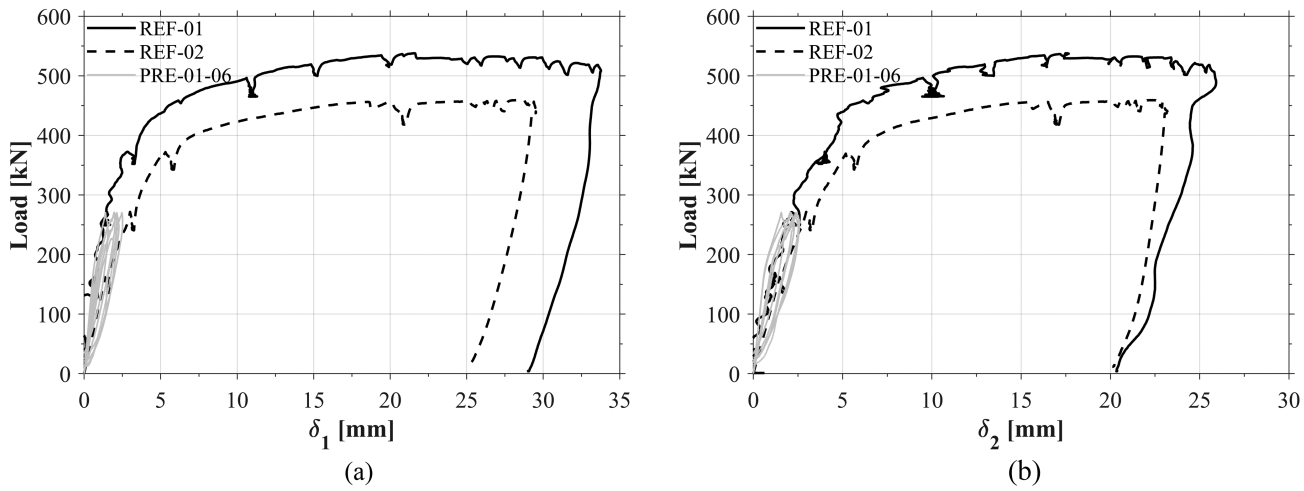

FIGURE 11 Load–vertical displacement curves of reference and pre-damaged specimens: δ_1 (a) and δ_2 (b). REF-01 curves were affected by a signal noise, partially removed by filtering the data.

3.3 | Application of FRCM layers

As mentioned, once the pre-damage (PRE) tests were carried out, the dapped-ends were retrofitted with the FRCM composites. The reinforcement layers were characterized by a nominal thickness of 20 mm, covering the first 1.3 m of the beam from the end of each dapped-end (Figure 9). A preliminary hydro-scarification of the concrete substrate on both sides of the beam specimens was performed with a water pressure of about 1000–1200 atm

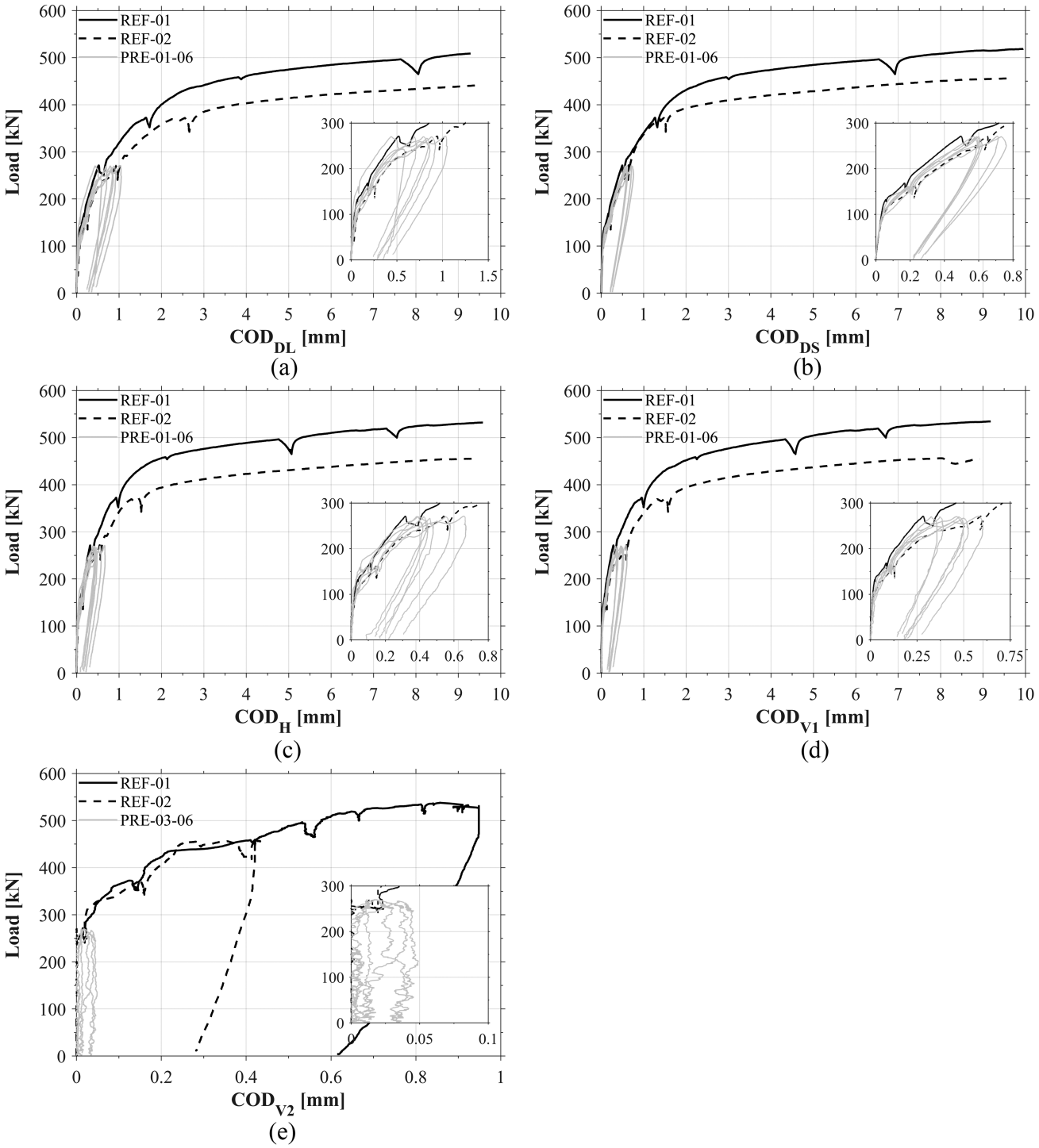

FIGURE 12 Load–COD curves of reference and pre-damaged specimens: COD_{DL} (a), COD_{DS} (b), COD_{H} (c), COD_{V1} (d), and COD_{V2} (e). All the curves are plotted within the instruments measuring range. Note that COD_{V2} signals of PRE-01 and PRE-02 tests were discarded due to incorrect readings and the results from the remaining tests were filtered to remove the signal noise. COD, crack opening displacement.

(as for the single lap shear tests) to prevent the delamination of the reinforcement from the support (Figure 10a). Then, the FRCM composite was applied following a typical hand lay-up technique: (i) application of the first mortar layer; (ii) placing of the AR-glass fabric (Figure 10b,c); and (iii) cast of the finishing mortar layer (Figure 10d). At the end of the tests, a series of cylinders (diameter 80 mm) was drilled from the beams. In

TABLE 10 Experimental results of reference and pre-damaged specimens: cracking load, batch reference, and stroke-COD values at $P = 270$ kN.

Specimen	Batch no.	Cracking load P_{crack} (kN)	Displacement values at $P_{pre} = 270$ kN δ_1 (mm)	δ_2 (mm)	COD_{DL} (mm)	COD_{DS} (mm)	COD_H (mm)	COD_{V1} (mm)	COD_{V2} (mm)
REF-01	1	132.96	1.44	2.56	0.67	0.56	0.41	0.35	0.02
REF-02		120.55	3.36	3.46	1.02	0.68	0.59	0.62	0.02
PRE-01		111.29	1.96	2.07	1.03	0.71	0.66	0.58	0.03
PRE-02		105.03	1.39	1.57	0.54	0.57	0.39	0.33	0.00
PRE-03	2	106.47	2.12	2.38	0.83	0.59	0.46	0.50	0.03
PRE-04		107.58	2.14	2.11	0.69	0.59	0.42	0.37	0.01
PRE-05		97.36	2.47	2.37	0.88	0.73	0.55	0.47	0.02
PRE-06		104.62	1.99	2.39	0.79	0.60	0.39	0.46	0.02

Abbreviation: COD, crack opening displacement.

TABLE 11 Experimental results of reference and retrofitted specimens: cracking load, maximum applied load, and relevant vertical displacements.

Specimen	Cracking load P_{crack} (kN)	Peak load P_{max} (kN)	Vertical displacement at P_{max} $\delta_{1(peak)}$ (mm)	$\delta_{2(peak)}$ (mm)	Ultimate vertical displacement $\delta_{1(final)}$ (mm)	$\delta_{2(final)}$ (mm)
REF-01	132.96	537.96	21.55	17.51	33.59	25.83
REF-02	120.55	459.29	28.49	22.36	29.38	22.93
RTF-(0°)-01	14.71	568.78	17.95	15.22	29.21	23.03
RTF-(0°)-02	12.26	530.20	14.65	12.83	22.05	17.98
RTF-(45°)-01	12.24	532.24	13.42	12.06	24.30	19.70
RTF-(45°)-02	12.92	530.71	15.51	14.02	21.84	17.31
RTF-(0° + 45°)-01	14.83	572.35	10.33	10.04	32.47	24.86
RTF-(0° + 45°)-02	15.13	540.51	10.22	9.49	25.72	22.19

Table 9, the measured thickness of both the front/back FRCM layer and the total one (concrete + front and back FRCM) are reported.

4 | EXPERIMENTAL RESULTS

In this section the results of the experimental tests are presented. To better understand the reported graphs, it is important to highlight the following aspects:

- All the reported curves correspond to the average values between the measurements on the front and the back sides of the specimens. This was done after verifying the symmetry of the data.
- Potentiometric transducers were characterized by a maximum range of 10 mm. Therefore, the curves are plotted up to the reaching of the maximum range and the end of the curve does not correspond to the end of the tests.
- The crack pattern was visually identified and marked with different colors on the beam surface at different load thresholds (P equal to 160, 270, 370, 450 kN) and at the end of the test (after the unloading phase). Due to the fact that the tests were stopped during the tracing of cracks, a limited reduction of load, due to relaxation effects, can be noticed in all the curves in correspondence to these phases.

4.1 | Reference and pre-damaged dapped-ends

The comparison between the response of the two reference (REF) and the six pre-damaged (PRE) dapped-ends is reported in Figure 11 and Figure 12 in terms of load

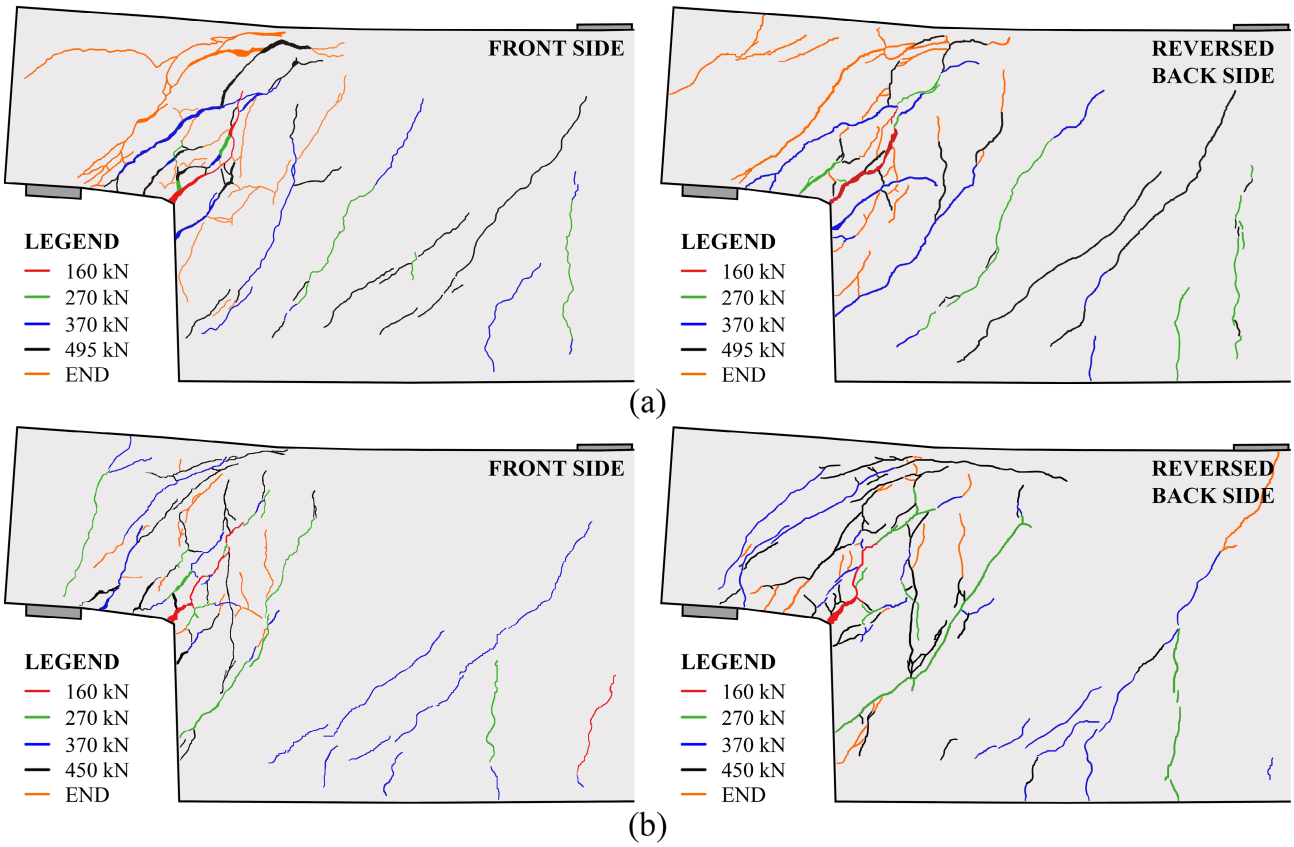

FIGURE 13 Crack pattern of reference specimens at different load stages: REF-01 (a) and REF-02 (b).

versus vertical displacement (δ_1 and δ_2) and load versus COD, respectively. The maximum load, P_{max}, recorded in the REF-01 test was 537.96 kN, corresponding to vertical displacements δ_1 and δ_2 respectively equal to 21.55 mm and 17.51 mm (Figure 11 and Table 11). A 15% lower load-bearing capacity (P_{max} = 459.29 kN) and higher values of the corresponding vertical displacements (δ_1 = 28.49 mm, and δ_2 = 22.36 mm) were encountered in case of REF-02. When looking into detail the load versus displacements curves from the reference tests (REF), the lower stiffness at the beginning of the REF-02 response might be attributed to the pre-damaged condition. On the other hand, the difference between the reference curves after the rebar yielding (Figure 12) is probably due to the load introduction schemes adopted in the two tests. In particular, in the REF-01 loading device the greater distance between the relative centre of rotation and the point of load application than in the other tests (Figure 8) could allow unintended tilting of the introduced load, thus inducing an additional confinement effect. With the aim of comparing the response of specimens tested with the same loading device, the results of REF-01 will be excluded from the discussion. Regarding the pre-damage tests, except for the COD_{V2}, all the COD curves show a significant residual crack opening (around 0.2–0.3 mm) after the unloading branch. Despite the good repeatability of the shape of the pre-damage curves (PRE-01 to 06) noticed in Figure 12, some variation in terms of maximum and residual COD_{DL} and COD_H values were observed. The effect on these differences on the behavior of retrofitted members will be discussed in the following sections.

In Table 10 the values of COD and vertical displacements measured at the pre-damage load (P_{PRE} = 270 kN) are reported for the reference and the pre-damaged dapped-ends, together with the load at which the first crack occurred at the inner corner of the dapped-end (P_{crack}). The obtained values of P_{crack} ranged between 97.36 and 132.96 kN and resulted to be in line with the mechanical properties of concrete coming from different batches (e.g., lower cracking loads were encountered in case of beams cast in the second batch, PRE-03 to 06). The cracking of the REF specimens (REF-01/02) was reached at load values of about 25% of their corresponding peak loads (Table 11).

The evolutions of the crack patterns of reference and pre-damaged specimens are shown in Figure 13 and Figure 14, respectively. In all cases, the first crack occurred at the inner corner (red lines), followed by the

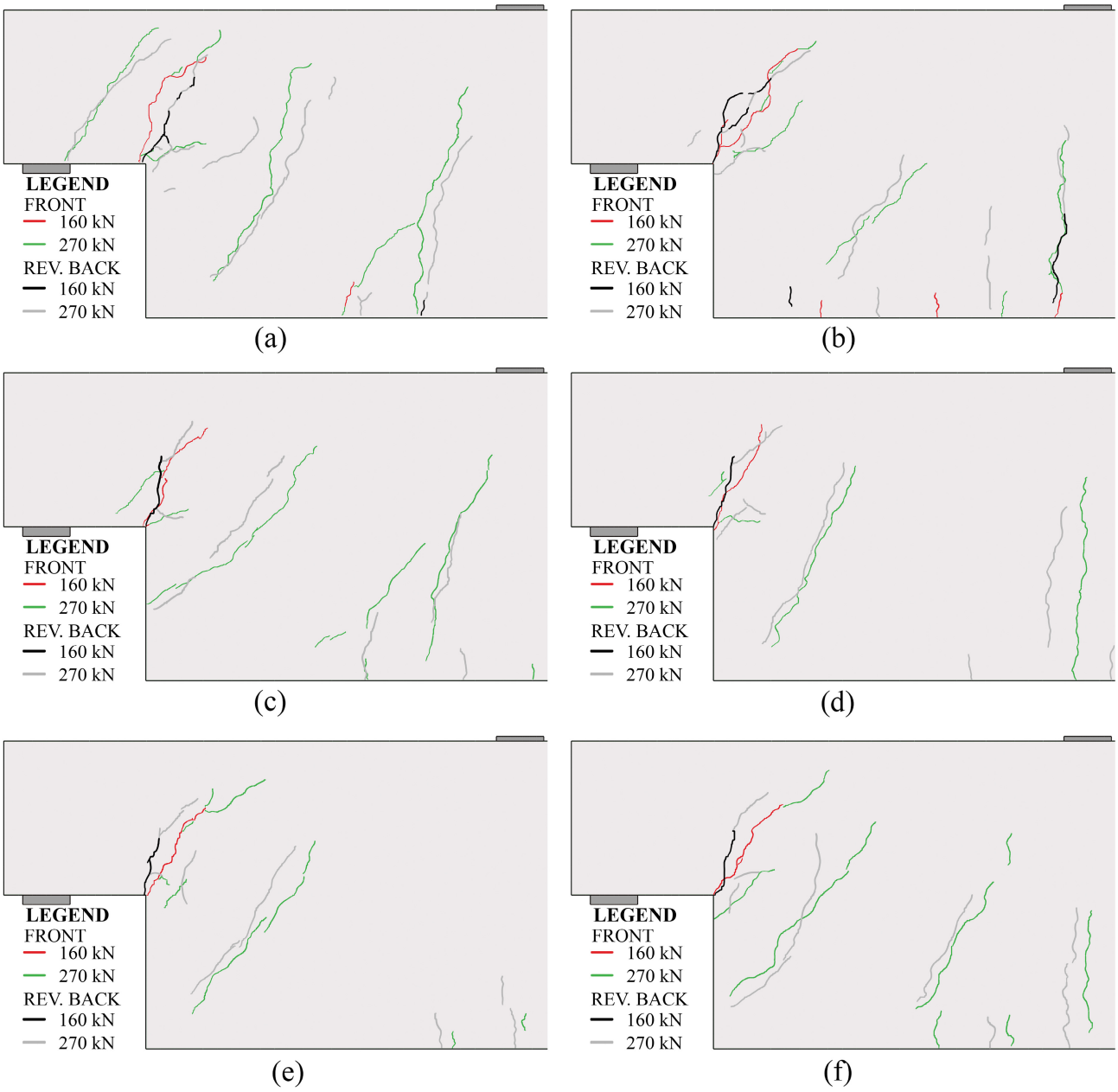

FIGURE 14 Crack pattern of pre-damaged specimens at different load stages: PRE-01 (a), PRE-02 (b), PRE-03 (c), PRE-04 (d), PRE-05 (e), and PRE-06 (f). Front and reversed back sides are depicted together.

development of flexural cracks at the bottom section of the beam (green lines). As the applied load increased, shear cracks (blue-black-orange lines) gradually developed in the full-depth section up to the failure of the nib. Some differences between the front- and the back-crack patterns were visible only at loads larger than 370 kN (Figure 13). The obtained crack patterns were aligned with those reported by other authors considering orthogonal[30] and combined[31] reinforcement. It is interesting to notice the fact that only inclined cracks developed in the nib area. This is an indicator that the dowel action contribution of the longitudinal reinforcement (3Φ12) was irrelevant,[32] even at larger vertical displacement, most probably due to the absence of vertical stirrups in the nib.

4.2 | Prediction of the load bearing capacity of REF dapped-end specimens with the use of strut-and-tie models

Considering that the experimental program comprised the pre-damaging of specimens before the application of the retrofitting solution, the question of the load value

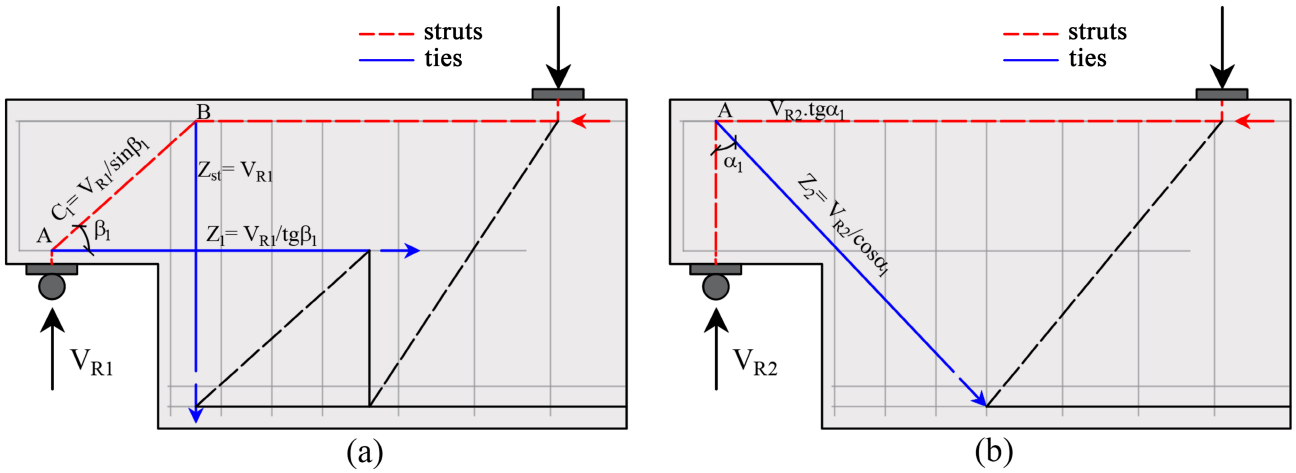

FIGURE 15 Strut-and-tie models adopted for the prediction of the load bearing capacity: first-orthogonal- (a) and second-diagonal- (b) resisting mechanisms.

TABLE 12 Load bearing capacity prediction of the REF dapped-end with strut-and-tie models.

Steel strength	f_{yd}			f_{yk}			$f_{y,av}$		
Number of stirrups	$V_{R,1}$ (kN)	$V_{R,2}$ (kN)	$P_{R,fyd}$ (kN)	$V_{R,1}$ (kN)	$V_{R,2}$ (kN)	$P_{R,fyk}$ (kN)	$V_{R,1}$ (kN)	$V_{R,2}$ (kN)	$P_{R,fyav}$ (kN)
1	61.47	85.19	219.98	70.69	97.97	252.98	82.70	110.53	289.84
2	119.26	85.19	306.70	137.15	97.97	352.67	161.59	110.53	408.20
3	101.46	85.19	280.00	116.68	97.97	321.96	137.47	110.53	372.00
4	88.28	85.19	260.20	101.52	97.97	299.23	119.62	110.53	345.22

Abbreviation: REF, reference specimen.

up to which subject the specimens arose. Therefore, a preliminary estimation of the load bearing capacity of the dapped-end was carried out by applying the simplified strut-and-tie approach. The geometry of the specimen and the steel layout described in Section 3.2 were considered for the identification of the simplified models (Figure 15). In particular, the combination of an orthogonal (Figure 15a) and a diagonal (Figure 15b) resisting mechanism was adopted, assuming that each one provides its full bearing capacity at the onset of yielding of each mechanism, without taking into account any coupling penalization, as suggested in the literature.[4]

The maximum stress in the concrete struts and the steel ties was computed assuming: (i) the design (f_{cd}, f_{yd}), (ii) the characteristic (f_{ck}, f_{yk}), or (iii) the average compressive/yielding strength experimentally obtained (f_{cm}, $f_{y,av}$). It is worth to note that both characteristic and design values were defined starting from the material classes (concrete C40/50, corresponding to batch n.1, and steel B450C grade). For the orthogonal model (Figure 15a), the number of stirrups involved in the equilibrium may vary from a minimum of 1 to a maximum of 4 according to the reinforcement layout. As example, in Figure 15a the schematic representation of the equilibrium considering only two stirrups is shown. Under this assumption, the value of the maximum reaction of each mechanism (V_{R1}, V_{R2}) resulted to be associated with the tensile failure of a tie, provided the fulfillment of all the compression checks. The maximum load that can be applied to the beam specimen (P_R) was then determined according to Equation (1), based on the resisting load of the single dapped-end ($V_{R1} + V_{R2}$) and the static scheme of the test (see Figure 6a).

$$P_R = \frac{3}{2}(V_{R1} + V_{R2}). \quad (1)$$

In Table 12, the computed V_{R1}, V_{R2}, and the maximum load (P_R) are reported considering both the variation of the number of stirrups involved in the orthogonal mechanism, and the steel strengths. For the pre-

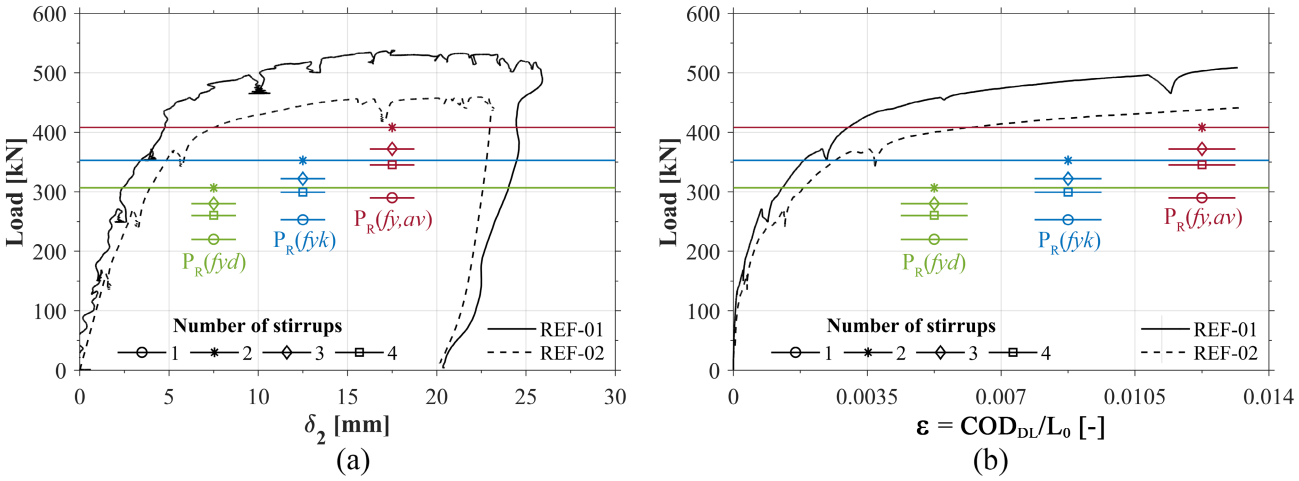

FIGURE 16 Comparison between experimental results (REF-01/02) and the analytical prediction of maximum load: load–vertical displacement δ_2 curves (a) and load–strain in correspondence to COD_{DL} curves (b). COD, crack opening displacement.

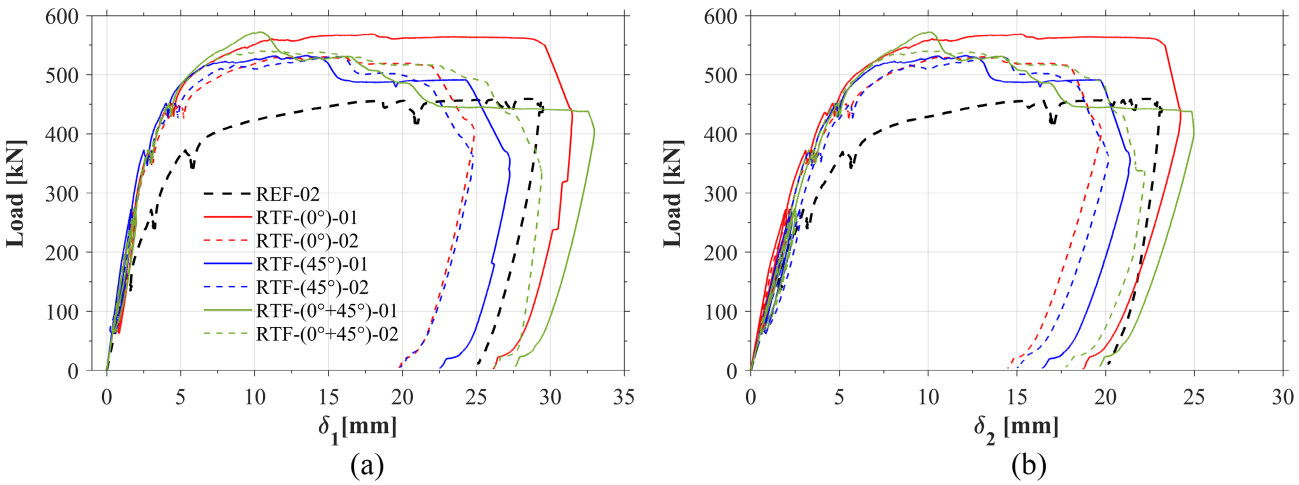

FIGURE 17 Load–vertical displacement curves of reference and retrofitted beams: δ_1 (a) and δ_2 (b). REF-01 curves were affected by a signal noise, partially removed by data filtering.

damaging of the specimens, the average between the design load values obtained varying the number of involved stirrups ($P_{R,fyd}$) was adopted (P_{PRE} = 270 kN). This choice represented an estimation at the ULS and it ensured a damage condition corresponding to the one possibly reached by a real dapped-end over its service life. From the results it can be noticed that the maximum bearing capacity was obtained for the case in which two stirrups were involved in the equilibrium, corresponding to an inclination of the strut β_1 equal to 41.93°.

Figure 16 illustrates the comparison between the strut-and-tie estimation and the experimental results obtained from specimens REF-01 and REF-02. As expected, a significant underestimation of the maximum load is obtained when considering design values, with a safety factor ($P_{EXP}/P_{R,fyd}$) equal to 1.75 with respect to specimen REF-01 and 1.50 with respect to REF-02. On the other hand, considering the characteristic ($P_{R,fyk}$) and the average steel strengths ($P_{R,fy,av}$), the load values are in good agreement with those in which a change of slope was experimentally obtained, thus validating the assumption of the yielding of the rebars.

4.3 | Retrofitted dapped-ends

The structural response of the reference specimen (REF-02) and of the retrofitted (RTF) samples are compared in Figure 17 and Figure 18. It is worth to note that in order to avoid any confusion that may arise from comparing tests carried out with different experimental setups (i.e., loading device), only REF-02 dapped-end is

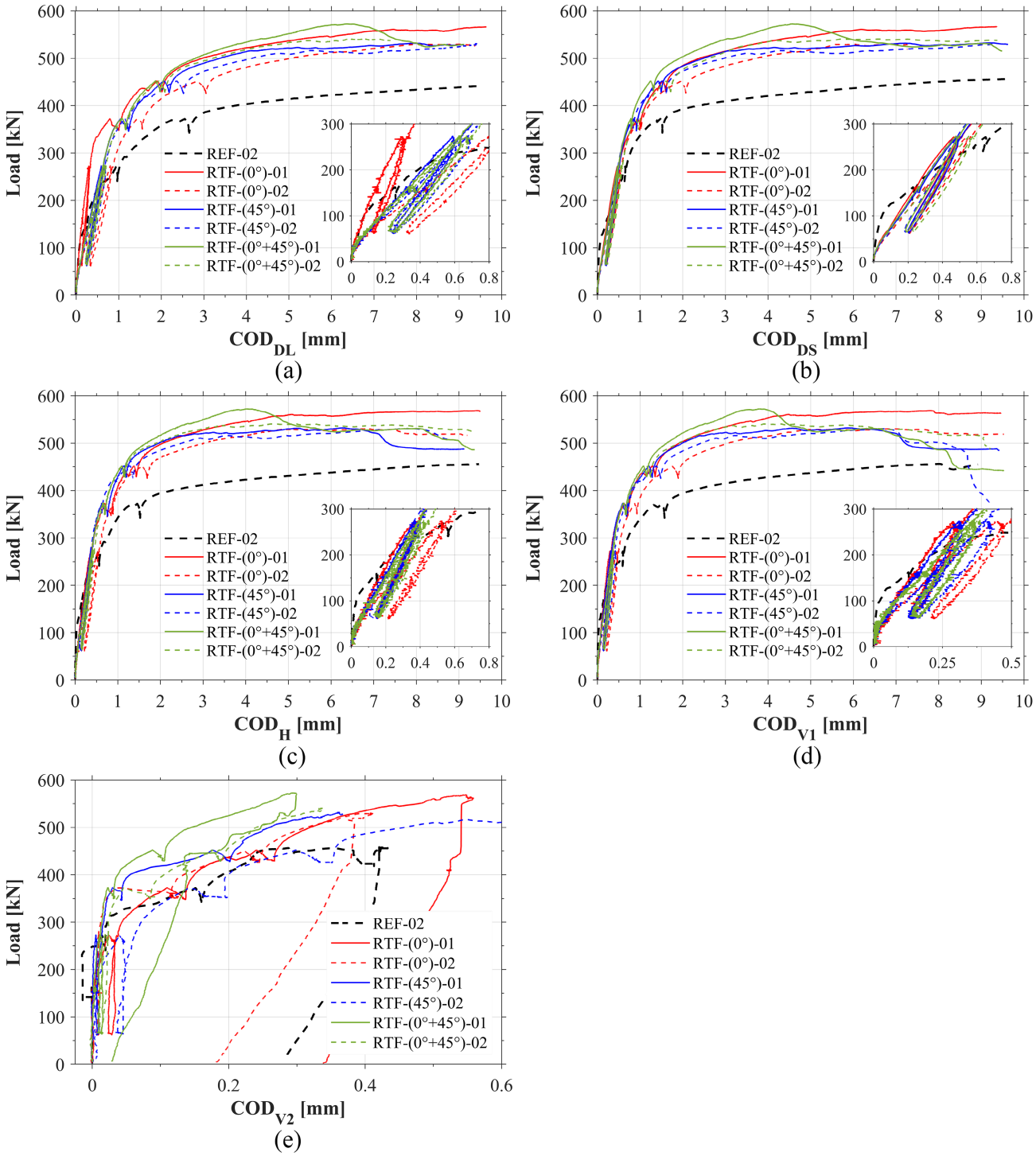

FIGURE 18 Load–COD curves of reference and retrofitted beams: COD_{DL} (a), COD_{DS} (b), COD_{H} (c), COD_{V1} (d), and COD_{V2} (e). COD, crack opening displacement.

used in the following comparisons. In all the graphs, solid lines refer to the first dapped-end tested for each beam, while dashed ones correspond to the second specimen. Assuming a possible increase of the maximum load bearing capacity of the retrofitted beams, the test procedure was changed as follows, not to risk exceeding the maximum capacity of the load cells placed underneath the dapped-end support (200 kN each). In the initial phase the stroke was increased until a load of 270 kN was reached (to be consistent with the pre-damage tests), then the specimens were unloaded to about 60 kN (unloading phase in curves of Figure 17 and Figure 18) and the load cells were by-passed. Subsequently, the tests were restarted and driven to failure.

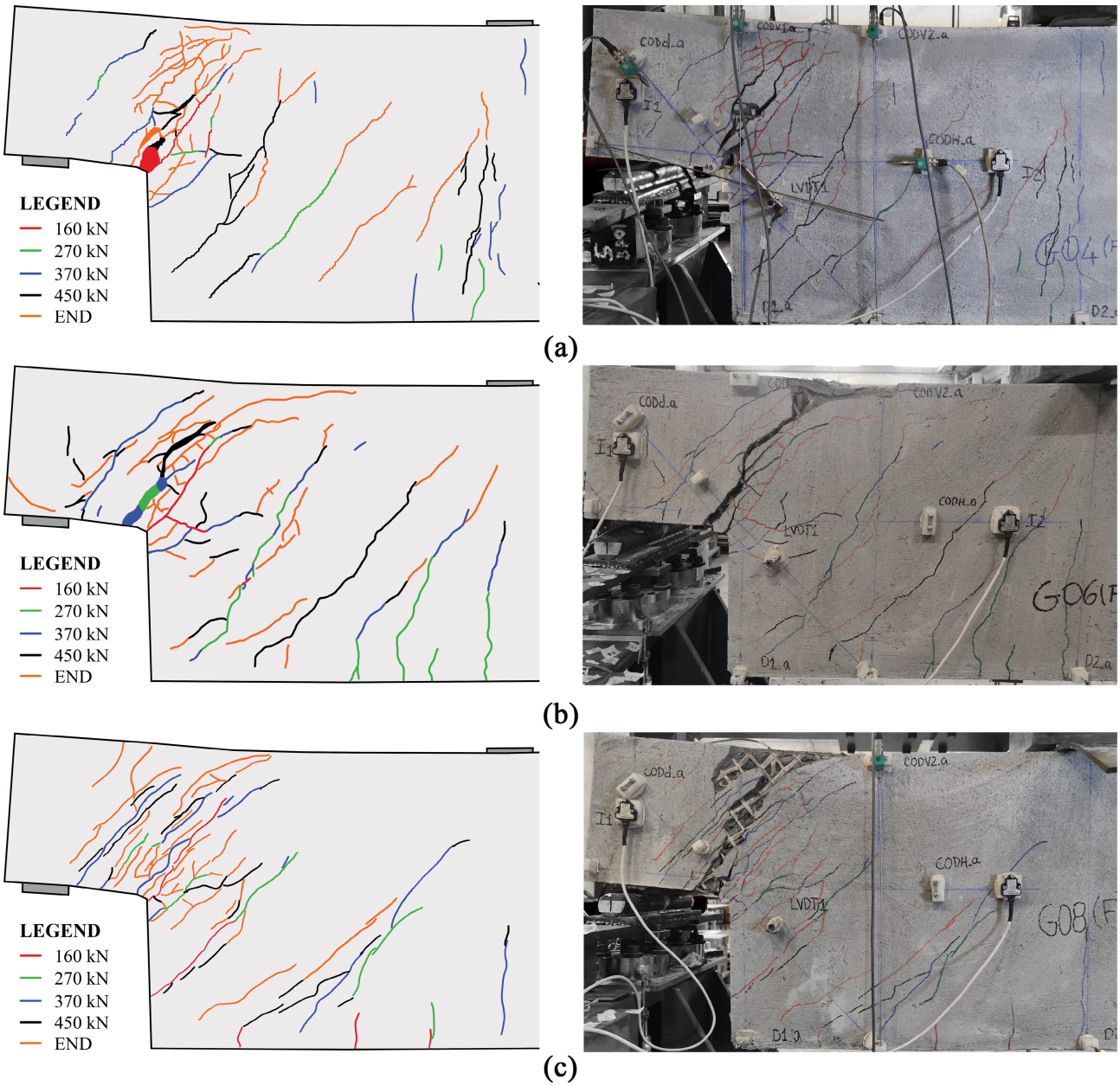

FIGURE 19 Crack patterns of retrofitted specimens at different load stages: RTF-(0°)-01 (a), RTF-(45°)-01 (b), and RTF-(0° + 45°)-01 (c). Only front side is depicted.

The average between the maximum loads registered in the 01/02 dapped-ends was equal to 549.49 kN, 531.48 kN, and 556.43 kN for specimens RTF-(0°), RTF-(45°), and RTF-(0° + 45°), respectively (Table 11). This corresponded to an increment of about 15%–21% with respect to the REF-02 response. It is interesting to notice that the use of two crossed fabric layers (0° + 45°) did not lead to a load increase equal to the sum of the two contributions obtained by using the layers separately, entailing a lower exploitation of the retrofitting capacity. The values of ultimate vertical displacements ($\delta_{1(\text{final})}$ and $\delta_{2(\text{final})}$) reported in Table 11, associated to the point at which a sudden reduction of load took place and after which the specimens were unloaded, were selected as the end of the tests (Figure 17).

In Table 11, the cracking loads measured in the RTF tests are reported. Comparing these values with the REF/PRE ones, it is possible to notice that they are in line with the FRCM layer thicknesses (Table 9) and the tensile strength of the repair mortar (see Section 2.3.1).

Figure 19 and Figure 20 show the crack patterns obtained from the test of the retrofitted dapped-ends. No textile delamination was observed, even if no connectors were introduced. All the specimens, including the

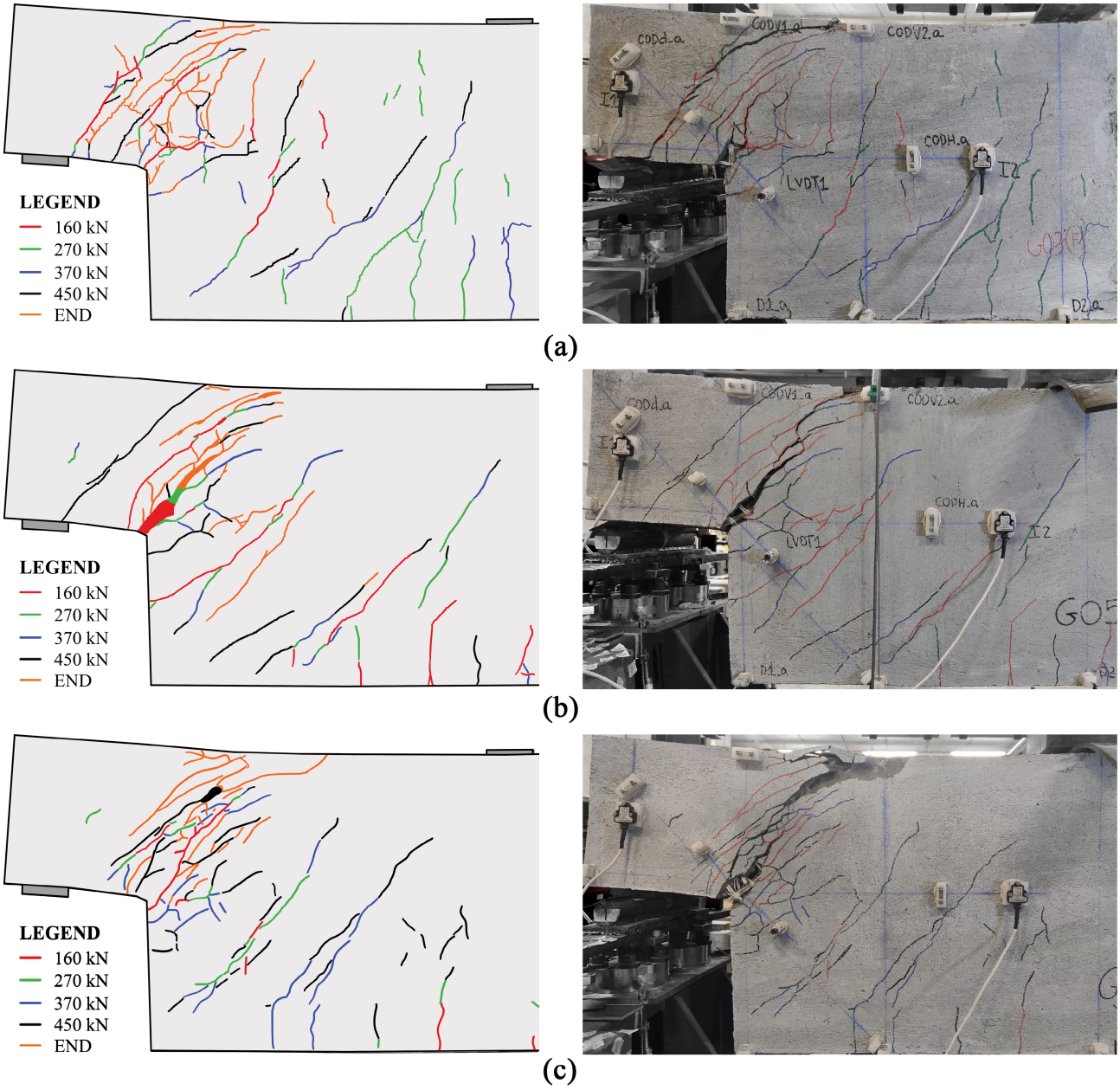

FIGURE 20 Crack patterns of retrofitted specimens at different load stages: RTF-(0°)-02 (a), RTF-(45°)-02 (b), and RTF-(0° + 45°)-02 (c). Only front side is depicted.

reference one (Figure 13), failed due to the crushing of the inclined concrete strut in correspondence to the top reinforcement, except for the case of specimen RTF-(0°)-01. In the latter the failure was governed by the rupture of the steel bars (one leg of the U-shaped horizontal bars on the front side, and one leg of the stirrup closer to the nib on the back side, see Figure 19a and Figure 21). The difference in the failure mode and the uneven behavior of the RTF-(0°)-01, as visible from the curves plotted in Figure 17 and Figure 18, are discussed in the following section.

5 | DISCUSSION AND INTERPRETATION OF THE RESULTS

Looking at the peak loads (P_{max}) reported in Table 11, it is possible to notice a good repeatability in the tests presenting the same type of retrofitting (tests 01 vs. tests 02), with COV smaller than 7%. It means that no significant effects are introduced by testing up to failure one dapped-end at the instance in which the other one already failed. Hence, the load bearing capacity of each retrofitting

FIGURE 21 Detail of the rebar rupture in specimen RTF-(0°)-01 after concrete demolition: failure of the U-shaped horizontal bar on the front side (a), and of the first stirrup on the back one (b). Note that the latter view is reversed.

TABLE 13 Experimental results of reference and retrofitted specimens: COD values at different load stages.

Specimen	Load stage (kN)	COD_{DL} (mm)	COD_{DS} (mm)	COD_{H} (mm)	COD_{V1} (mm)	COD_{V2} (mm)
REF-02	160	0.25	0.22	0.14	0.12	0.00
	270	0.93	0.64	0.54	0.59	0.01
	370	2.52	1.45	1.44	1.49	0.15
	450	–[a]	7.89	7.81	6.60	0.25
RTF-(0°)-01/02	160	0.14/0.43	0.24/0.29	0.18/0.28	0.15/0.22	0.00/0.00
	270	0.28/0.80	0.46/0.53	0.36/0.52	0.29/0.44	0.02/0.01
	370	0.77/1.41	0.92/0.97	0.68/0.86	0.61/0.85	0.11/0.03
	450	1.87/2.81	1.51/1.93	1.36/1.55	1.26/1.74	0.24/0.22
RTF-(45°)-01/02	160	0.32/0.37	0.26/0.26	0.21/0.24	0.16/0.22	0.00/0.00
	270	0.58/0.67	0.48/0.47	0.36/0.42	0.30/0.41	0.01/0.01
	370	1.03/1.12	0.84/0.79	0.62/0.90	0.58/0.67	0.03/0.03
	450	2.03/2.31	1.40/1.49	1.10/1.59	1.19/1.35	0.17/0.14
RTF-(0° + 45°)-01/02	160	0.33/0.36	0.25/0.30	0.21/0.23	0.18/0.19	0.00/0.00
	270	0.62/0.66	0.47/0.55	0.40/0.41	0.35/0.35	0.01/0.02
	370	1.03/1.06	0.77/0.89	0.63/0.66	0.60/0.59	0.02/0.04
	450	1.84/1.92	1.23/1.59	1.07/1.08	1.06/1.14	0.09/0.18

Abbreviation: COD, crack opening displacement.
[a]Instruments lost during the test.

solution can be associated to the average value between the peak loads of the first and the second tests.

With respect to the reference specimen (REF-02), the average load bearing capacity was increased by 19.6% when the fabric was oriented at 0°, by 15.7% when oriented at 45°, and by 21.2% when the two solutions were combined. Moreover, due to the lower ultimate strain of the FRCM system with respect to the one of the steel bars, the maximum load bearing capacity of the RTF beams, which coincided with the rupture of the glass fabric, corresponded to a vertical deflection lower than the one at the peak of the REF tests. Since the yielding point on the overall response curve seems not to be affected by the presence of the FRCM reinforcement (similar δ_y recorded in the REF-02 and the RTF cases), the decrease of the displacement at the failure, δ_u, leads to a slight

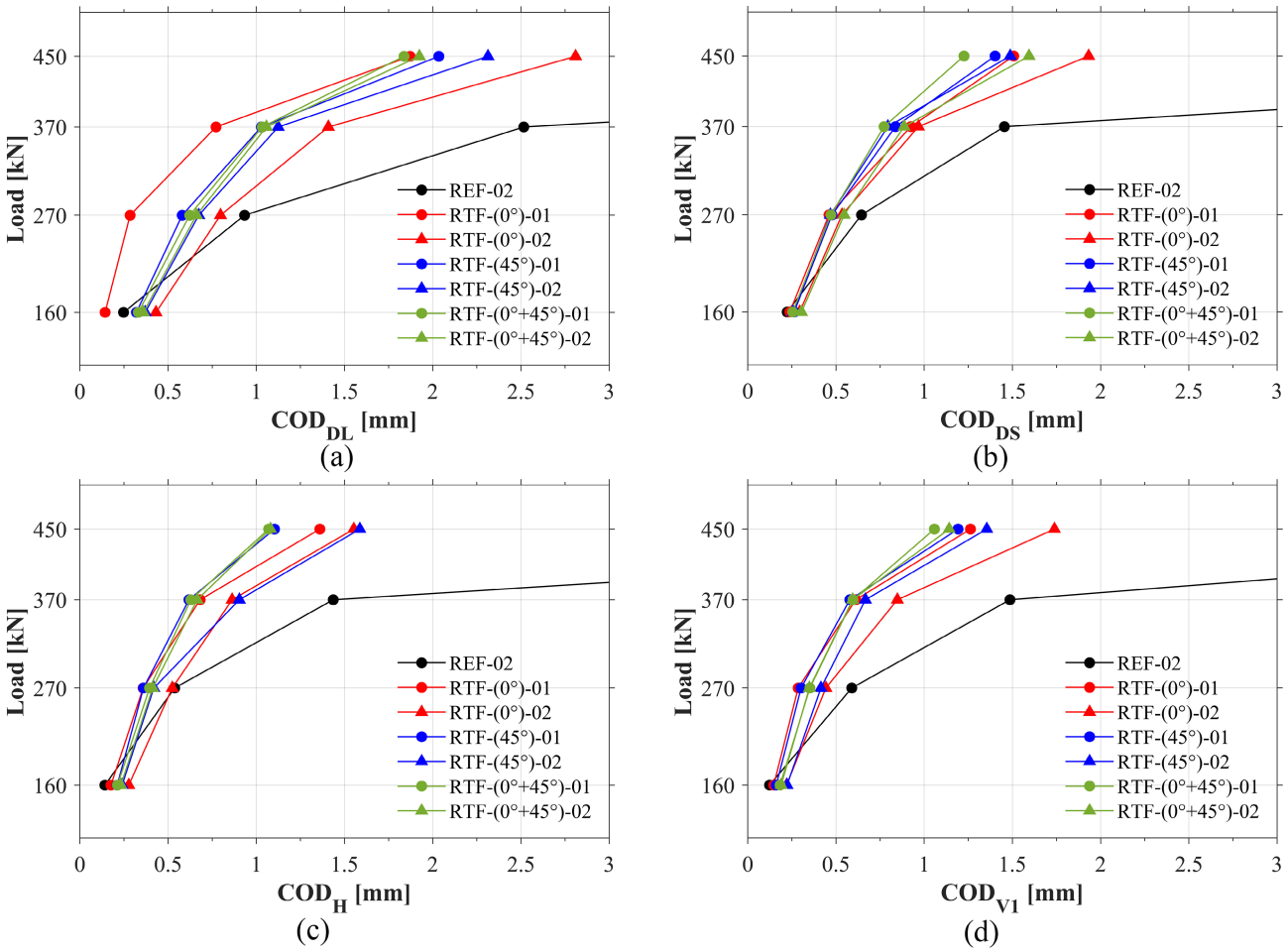

FIGURE 22 COD values at different load stages: COD_{DL} (a), COD_{DS} (b), COD_{H} (c), and COD_{V1} (d). COD, crack opening displacement.

reduction of ductility, defined as δ_u/δ_y. Due to this, to properly evaluate the effect of the FRCM retrofitting, it could be interesting to compare the recorded loads at the same vertical displacement. As an example, in case of RTF-(0° + 45°) dapped-ends, an average peak load of 556.43 kN was recorded at a δ_1 equal to around 10 mm, corresponding to an increase of about 30% with respect to the vertical load of the REF-02 registered at the same deflection (around 420 kN).

However, the contribution of the FRCM systems must not be exclusively measured in terms of increment in the load-carrying capacity, but also in terms of control of crack openings. To evaluate this effect, a comparison between the measured COD values of reference and retrofitted tests at different load stages (160, 270, 370, and 450 kN) is presented in Table 13 and Figure 22. The effect of the FRCM in controlling crack openings appeared significantly larger as the applied load increased due to the typical strain-hardening behavior of this composite. For example, the addition of the FRCM system can lead to a maximum reduction in crack openings of more than six times those registered in the reference test (e.g., COD_{DS} of 1.23 mm and 7.89 mm were respectively recorded for the specimens RTF-(0° + 45°)-01 and REF-02 at 450 kN).

Moreover, from Figure 22 it can be observed that, as expected, lower values of CODs were generally obtained for specimens retrofitted with two superimposed layers of AR-glass fabric, with respect to the cases in which only one layer was used. Regarding the comparison between the different fabric orientations, the application with the warp at 45° instead of 0° helped in controlling the opening of the diagonal cracks localized at the inner corner of the nib, as visible from the COD_{DS} values reported in Figure 22b. The same observation can be extended to the COD_{DL} measures, excluding the results of the RTF-(0°)-01. As demonstrated by Figure 23, the response of the latter was influenced by the discrepancies between the corresponding pre-damage behaviors. In fact, the PRE-02 (corresponding to RTF-(0°)-01) showed lower maximum and residual COD_{DL} and COD_{DS} values (Figure 23a,b), a stiffer curve in the un-loading phase (Figure 23b), and a higher concentration of cracks in the nib zone (Figure 23c,d) with respect to the PRE-01 (corresponding to RTF-(0°)-02).

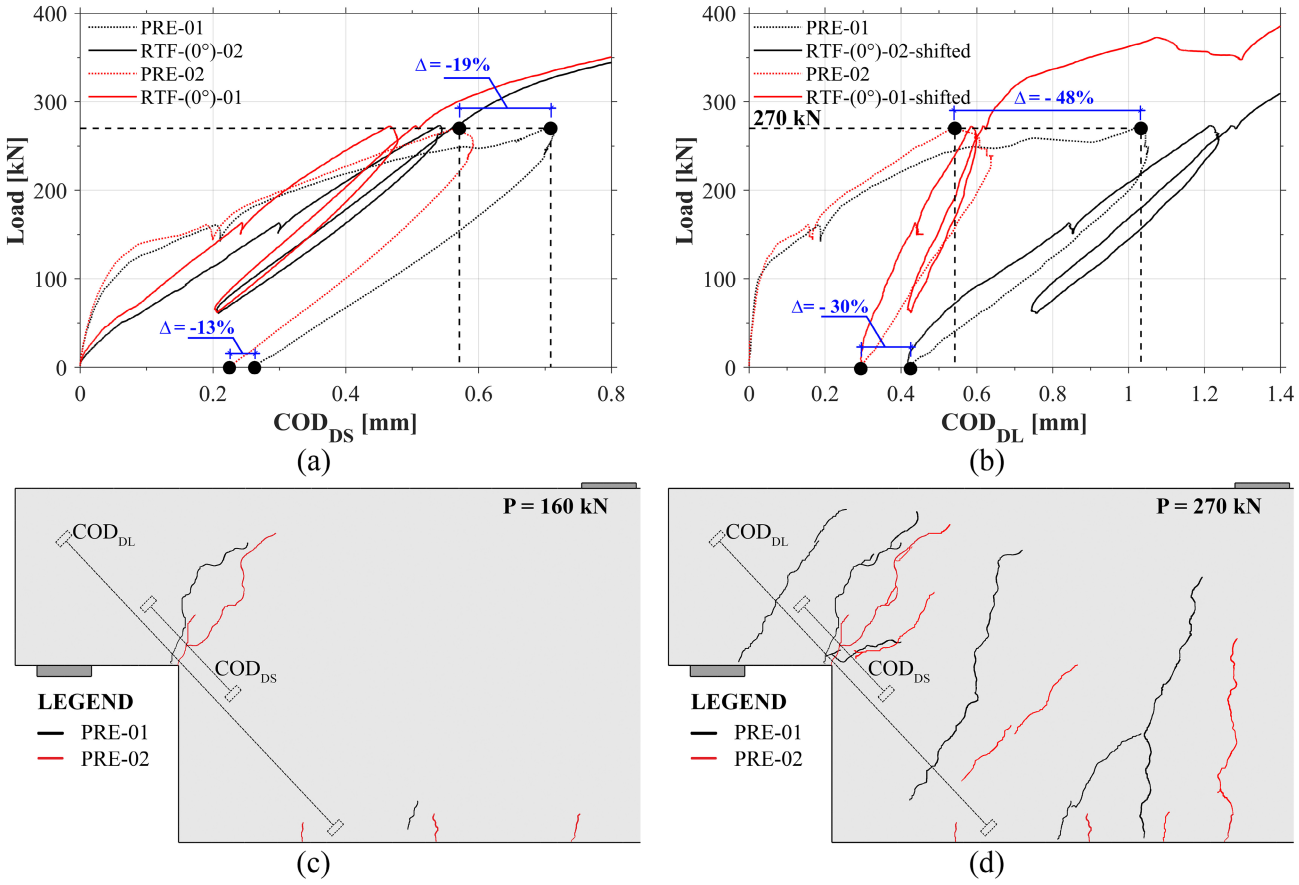

FIGURE 23 Comparison between PRE-01 (corresponding to RTF-(0°)-02) and PRE-02 (corresponding to RTF-(0°)-01) specimens in terms of: load–COD_{DS} curves (a), load–COD_{DL} curves (b), and front crack patterns at 160 kN (c), and 270 kN (d). COD, crack opening displacement.

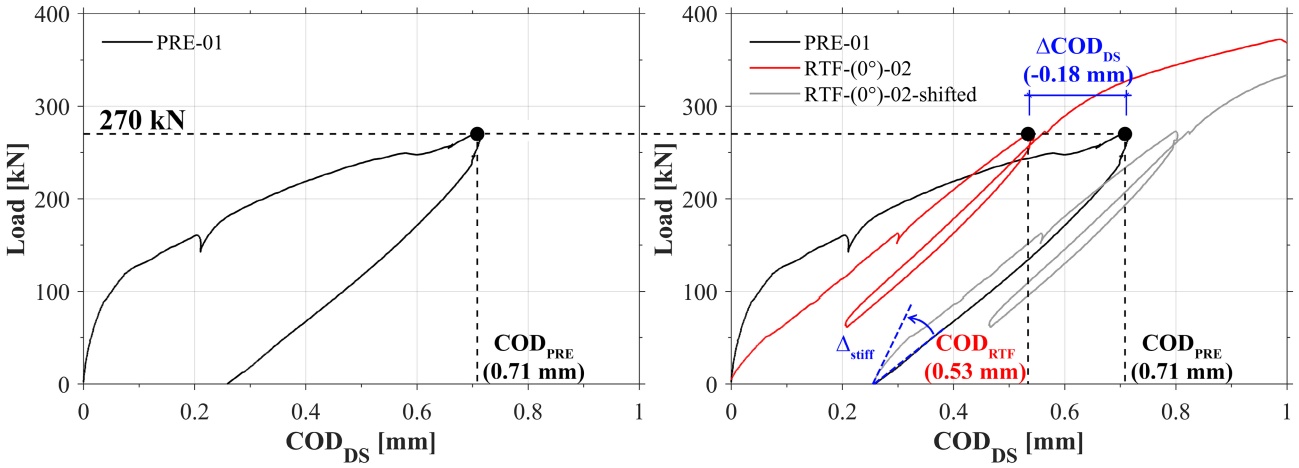

FIGURE 24 Example of the identification of the crack opening displacement variation, ΔCOD_{DS}, between the values recorded in the pre-damaging phase, COD_{PRE}, and on retrofitted dapped-ends, COD_{RTF}, at 270 kN. RTF-(0°)-02-shifted curve was introduced to highlight the partial stiffness recovery (Δ_{stiff}) with respect to the PRE-01 response.

The effect on the fabric orientation on the other CODs was less pronounced because the main crack orientation is the inclined one and due to the longer GLs considered (e.g. COD_H in case of the 0°-oriented fabric).

From Figure 22 it can also be noticed that, when the applied load was equal to 160 kN, the COD values recorded in the tests on retrofitted specimens were higher than the reference ones. This was clearly

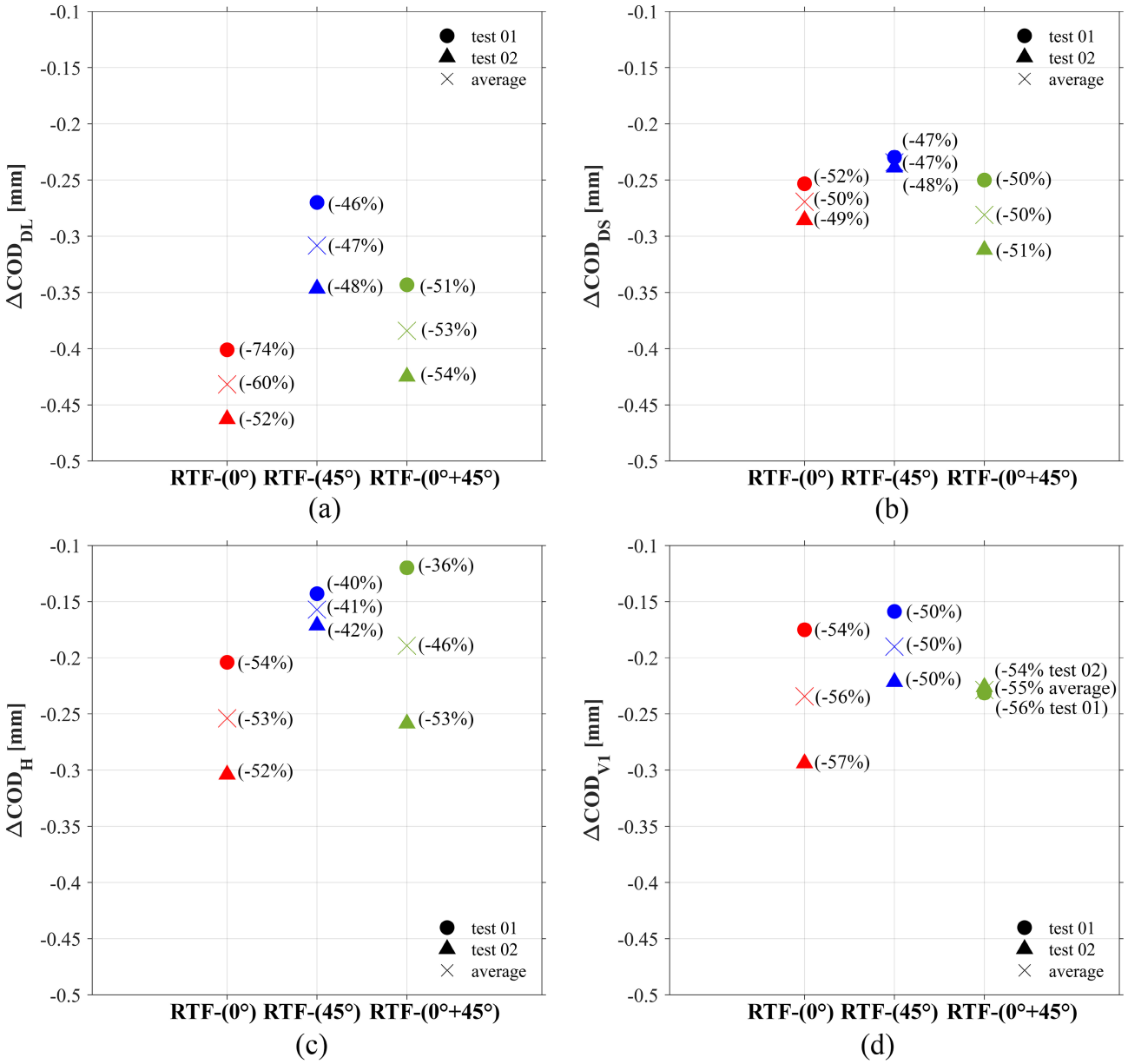

FIGURE 25 Comparison between the ΔCOD values computed at a load equal to 160 kN (RTF vs. PRE): ΔCOD_{DL} (a), ΔCOD_{DS} (b), ΔCOD_{H} (c), and ΔCOD_{V1} (d). COD, crack opening displacement.

associated to the existing damage prior to the retrofitting (see the residual crack openings at the end of the unloading phase in Figure 12). To better recognize the beneficial effect of the FRCM, it was decided to compare the COD values recorded in the retrofitted dapped-ends and in the pre-damage tests, computing the crack opening variation, ΔCOD, as shown in Figure 24 for the case of RTF-(0°)-02 test at 270 kN. The detail of the comparison, at a load equal to 160 kN and 270 kN is presented in Figure 25 and Figure 26, respectively (negative values corresponded to a reduction of opening in the RTF test with respect to the PRE). It can be noticed that the contribution of the FRCM to crack opening control was relevant, especially in case of diagonal cracks (COD_{DL} and COD_{DS}), resulting in ΔCOD ranging between 0.1 and 0.5 mm. The greater contribution was encountered at a load value of 160 kN (Figure 25), which can be associated to a serviceability design load and therefore to a more representative and repeatable state. In particular, an overall reduction in the crack openings of 51% was registered at 160 kN, in contrast with a 20% obtained at a load value of 270 kN (ultimate design load).

At the end, the effect on cracks development was also visible on the evolution of the crack pattern (Figure 19 and Figure 20). It can be observed how the cracks tend to

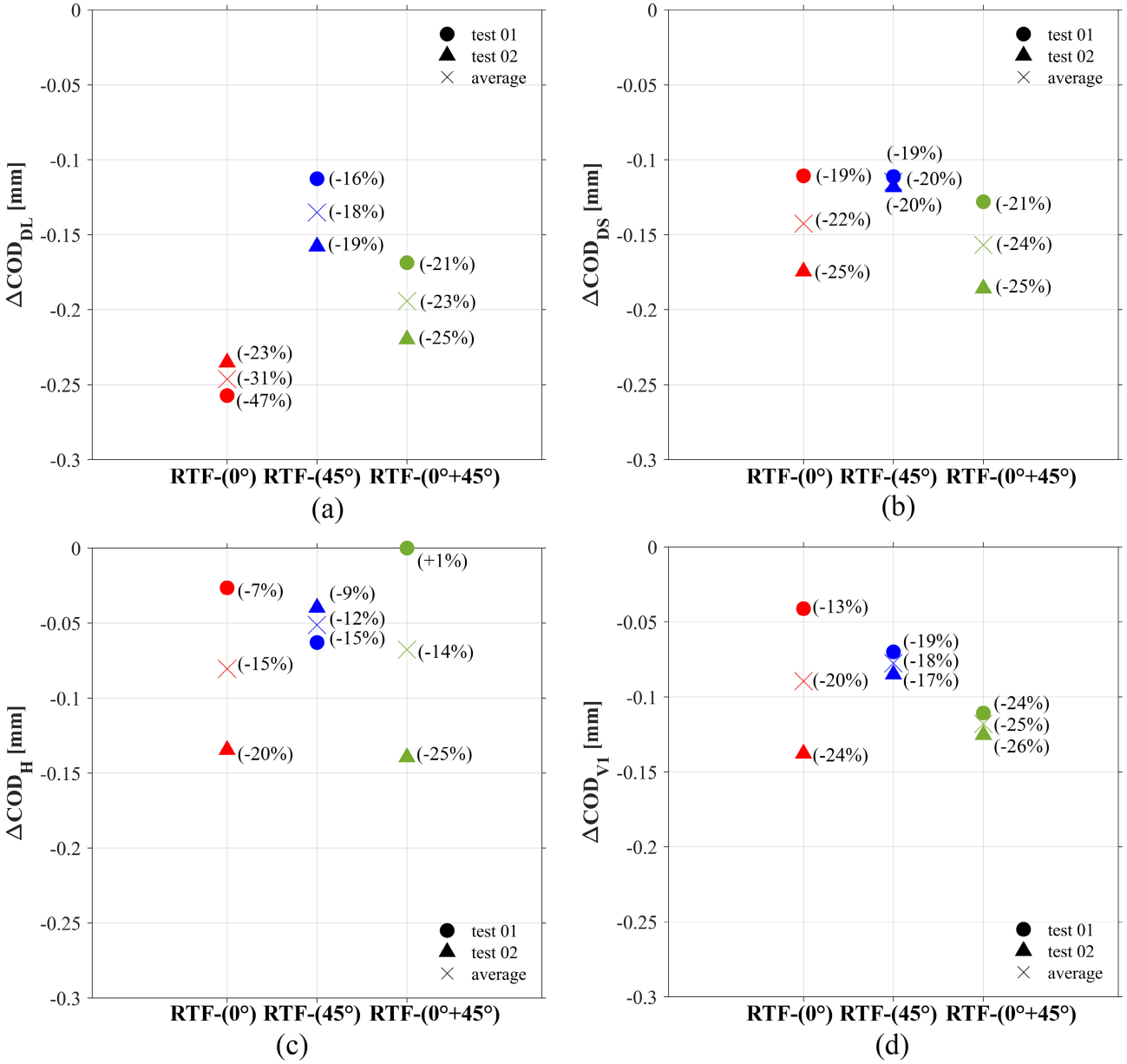

FIGURE 26 Comparison between the ΔCOD values computed at a load equal to 270 kN: ΔCOD_{DL} (a), ΔCOD_{DS} (b), ΔCOD_{H} (c), and ΔCOD_{V1} (d). COD, crack opening displacement.

develop mainly in a direction perpendicular to the warp wires (vertical in case of specimens RTF-(0°) and more inclined for RTF-(45°) dapped-ends). Moreover, in the cases in which the two directions were combined (RTF-(0° + 45°)) the cracks developed mostly in the inner corner of the nib.

Comparing the initial slope of the RTF response curves with both the beginning and the end of the pre-damage ones, it is possible to notice a partial recovery of the stiffness due to the application of the FRCM composite (e.g., Δ_{stiff} in the comparison reported in Figure 24 for the RTF-(0°)-02 test and its corresponding PRE-01 pre-damage test). This partial stiffness recovery is clearly influenced by both the sizes of the dapped-end and the thickness of the FRCM layers, so it should be considered with caution.

6 | CONCLUSIONS AND FURTHER DEVELOPMENTS

An extensive experimental campaign was carried out in order to evaluate the contribution of FRCM retrofitting systems on the structural performance of RC dapped-end beams, typically found in existing bridge structures from the 1950s to 1970s.

From the analysis of the experimental results, the following conclusions can be drawn:

- A good repeatability of the experimental data was encountered when the beams were reversed after testing the first dapped-end, validating the suitability of the adopted three-point non-symmetric bending test set-up. Therefore, it was possible to consider the average of the responses of the two dapped-ends of each single beam for comparison and discussion.

Regarding the effect of the FRCM retrofitting:

- An increment of the load-bearing capacity ranging between 15% and 21% with respect to the reference dapped-end was observed. This effect was more pronounced at a vertical displacement corresponding to the peak of the retrofitted curves (failure of the fabric).
- The load increment with respect to the reference capacity obtained with the application of two crossed fabric layers ($0^\circ + 45^\circ$) resulted lower than the sum of the individual contributions of each fabric orientation (0° and 45°). This led to a lower exploitation of the FRCM retrofitting capacity.
- Considering the most performing retrofitting solution (two superimposed layers), a reduction of the crack openings up to around six times those registered in the unretrofitted specimens was observed. This contribution appeared to be more relevant as the applied load increased due to the strain-hardening behavior of the composite. Moreover, it is important to highlight that this beneficial effect obtained in presence of residual preexisting cracks has a significant impact on the durability of the structural element.
- The direction of the warp wires had an influence on both crack patterns and crack openings. The choice to adopt a FRCM system with a particular orientation must consider the preexisting damage of the specimen. Better performance can be obtained placing the warp wires perpendicular to the main preexisting cracks.

The experimental results presented in this paper are part of a research program aimed at calibrating nonlinear numerical models and analyses for estimating the response of this type of structural element and, in particular, with reference to the estimation of the FRCM-retrofitted dapped-end beams behavior. In addition, further experimental tests will be performed to extend the investigation of the action of the composite reinforcement, considering the typical damage undergone by RC structures exposed to environmental effects (e.g., chloride ingress and oxidation of steel rebar).

ACKNOWLEDGMENTS

The authors would like to acknowledge Gavazzi Tessuti Spa and Master Builder Solution Italia for their precious contribution to the research.

FUNDING INFORMATION

The experimental research was financially supported by RELUIS WP14 – 2019/2021. The theoretical analysis was carried out in the framework of the financial support CSLLPP RELUIS Agreement DM 578/2020.

CONFLICT OF INTEREST STATEMENT

The authors declare no conflicts of interest.

DATA AVAILABILITY STATEMENT

The data that support the findings of this study are available from the corresponding author upon reasonable request.

ORCID

Katherina Flores Ferreira https://orcid.org/0000-0002-0371-504X
Marco Carlo Rampini https://orcid.org/0000-0002-6302-3037
Giulio Zani https://orcid.org/0000-0001-9794-7820
Matteo Colombo https://orcid.org/0000-0001-6457-7894
Marco di Prisco https://orcid.org/0000-0003-1779-2449

REFERENCES

1. Werner MP, Dilger WH. Shear design of prestressed concrete stepped beams. J Prestress Concr Inst. 1973;18(4):37–49. https://doi.org/10.15554/pcij.07011973.37.49
2. Mattock AH, Chan TC. Design and behavior of dapped-end beams. PCI J. 1979;24(6):28–45. https://doi.org/10.15554/pcij.11011979.28.45
3. Cook WD, Mitchell D. Studies of disturbed regions near discontinuities in reinforced concrete members. ACI Struct J. 1988;85(2):206–16. https://doi.org/10.14359/2772
4. Schlaich J, Schäfer K. Design and detailing of structural concrete using strut-and-tie models. Struct Eng. 1991;69(6):113–25.
5. Wang Q, Guo Z, Hoogenboom PCJ. Experimental investigation on the shear capacity of RC dapped end beams and design recommendations. Struct Eng Mech. 2005;21(2):221–35. https://doi.org/10.12989/sem.2005.21.2.221
6. Moreno JY, Meli R. Experimental study and numerical simulation of the behaviour of concrete dapped-end beams. Eng Model. 2013;26(1–4):15–25.
7. Desnerck P, Lees JM, Morley CT. Impact of the reinforcement layout on the load capacity of reinforced concrete half-joints. Eng Struct. 2016;127:227–39. https://doi.org/10.1016/j.engstruct.2016.08.061
8. Desnerck P, Lees JM, Morley CT. The effect of local reinforcing bar reductions and anchorage zone cracking on the load capacity of RC half-joints. Eng Struct. 2017;152:865–77. https://doi.org/10.1016/j.engstruct.2017.09.021

9. di Prisco M, Colombo M, Martinelli P, Coronelli D. The technical causes of the collapse of Annone overpass on SS.36. In: Proceedings of Italian Concrete Days; 2018.
10. Mitchell D, Marchand J, Croteau P, Cook WD. Concorde overpass collapse: structural aspects. J Perform Constr Facil. 2011;25(6):545–53. https://doi.org/10.1061/(asce)cf.1943-5509.0000183
11. Consiglio Nazionale delle Ricerche. CNR DT 215/2018: Guide for the design and construction of externally bonded fibre reinforced inorganic matrix systems for strengthening existing structures. ACI Comm 440. National Research Council; Published online; 2018. p. 144.
12. Consiglio Superiore dei Lavori Pubblici. Linea Guida per la identificazione, la qualificazione ed il controllo di accettazione di compositi fibrorinforzati a matrice inorganica (FRCM) da utilizzarsi per il consolidamento strutturale di costruzioni esistenti. Consiglio Superiore dei Lavori Pubblici; Published online; 2018. p. 1–43. https://doi.org/10.1109/ChiCC.2015.7260208
13. Koutas LN, Tetta Z, Bournas DA, Triantafillou TC. Strengthening of concrete structures with textile reinforced mortars: state-of-the-art review. J Compos Constr. 2019;23(1):1–20. https://doi.org/10.1061/(ASCE)CC.1943-5614.0000882
14. Ombres L. Structural performances of reinforced concrete beams strengthened in shear with a cement based fiber composite material. Compos Struct. 2015;122:316–29. https://doi.org/10.1016/j.compstruct.2014.11.059
15. Tetta ZC, Koutas LN, Bournas DA. Shear strengthening of concrete members with TRM jackets: effect of shear span-to-depth ratio, material and amount of external reinforcement. Compos Part B Eng. 2017;2018(137):184–201. https://doi.org/10.1016/j.compositesb.2017.10.041
16. Bielak J, Adam V, Hegger J, Classen M. Shear capacity of textile-reinforced concrete slabs without shear reinforcement. Appl Sci. 2019;9(7):1–20. https://doi.org/10.3390/app9071382
17. Rossi E, Randl N, Harsányi P, Mészöly T. Experimental study of fibre-reinforced TRC shear strengthening applications on non-stirrup reinforced concrete T-beams. Eng Struct. 2022;256:113923. https://doi.org/10.1016/j.engstruct.2022.113923
18. Nagy-György T, Sas G, Dâescu AC, Barros JAO, Stoian V. Experimental and numerical assessment of the effectiveness of FRP-based strengthening configurations for dapped-end RC beams. Eng Struct. 2012;44:291–303. https://doi.org/10.1016/j.engstruct.2012.06.006
19. Afefy HM, Sennah K, Cofini A. Retrofitting actual-size pre-cracked precast prestressed concrete double-tee girders using externally bonded CFRP sheets. J Perform Constr Facil. 2016;30(2):1–18. https://doi.org/10.1061/(asce)cf.1943-5509.0000763
20. Gemi L, Aksoylu C, Yazman Ş, Özkılıç YO, Arslan MH. Experimental investigation of shear capacity and damage analysis of thinned end prefabricated concrete purlins strengthened by CFRP composite. Compos Struct. 2019;229:111399. https://doi.org/10.1016/j.compstruct.2019.111399
21. CEB-FIP. Fib model code for concrete structures 2010. International Federation for Structural Concrete (FIB); 2013. https://doi.org/10.1002/9783433604090
22. British Standards Institution. Metallic Materials - Tensile Testing BS EN ISO 6892-1. 2019.
23. Rampini MC, Zani G, Colombo M, di Prisco M. Mechanical behaviour of TRC composites: experimental and analytical approaches. Appl Sci. 2019;9(7):1492. https://doi.org/10.3390/app9071492
24. Rampini MC, Zani G, Schouler L, Colombo M, di Prisco M. Effect of textile characteristics on the AR-glass fabric efficiency. Textiles. 2021;1(2):387–404. https://doi.org/10.3390/textiles1020020
25. Colombo IG, Magri A, Zani G, Colombo M, Di Prisco M. Erratum: Textile reinforced concrete: experimental investigation on design parameters. Mater Struct Constr. 2013;46(11):1953–71. https://doi.org/10.1617/s11527-013-0023-7
26. Carloni C, Verre S, Sneed LH, Ombres L. Loading rate effect on the debonding phenomenon in fiber reinforced cementitious matrix-concrete joints. Compos Part B Eng. 2017;108:301–14. https://doi.org/10.1016/j.compositesb.2016.09.087
27. Rampini MC, Zani G, Colombo M, di Prisco M. The role of concrete substrate roughness on externally bonded fabric-reinforced cementitious matrix (FRCM) layers. First Fib Italy YMG symposium on concrete and concrete structures. 2020;56–63.
28. Raoof SM, Koutas LN, Bournas DA. Bond between textile-reinforced mortar (TRM) and concrete substrates: experimental investigation. Compos Part B Eng. 2016;98:350–61. https://doi.org/10.1016/j.compositesb.2016.05.041
29. Leone M, Aiello MA, Balsamo A, Carozzi FG, Ceroni F, Corradi M, et al. Glass fabric reinforced cementitious matrix: tensile properties and bond performance on masonry substrate. Compos Part B Eng. 2017;127:196–214. https://doi.org/10.1016/j.compositesb.2017.06.028
30. Rajapakse C, Degée H, Mihaylov B. Investigation of shear and flexural failures of dapped-end connections with orthogonal reinforcement. Eng Struct. 2022;260:114233. https://doi.org/10.1016/j.engstruct.2022.114233
31. Mata-Falcón J, Pallarés L, Miguel PF. Proposal and experimental validation of simplified strut-and-tie models on dapped-end beams. Eng Struct. 2019;183:594–609. https://doi.org/10.1016/j.engstruct.2019.01.010
32. Dei Poli S, di Prisco M, Gambarova PG. Cover and stirrup effects on the shear response of dowel bar embedded in concrete. ACI Struct J. 1993;90(4):441–50. https://doi.org/10.14359/3962

AUTHOR BIOGRAPHIES

Katherina Flores Ferreira, Department of Civil and Environmental Engineering, Politecnico di Milano, Piazza Leonardo da Vinci, 32 - 20133 Milano, Italy. Email: katherina.flores@polimi.it

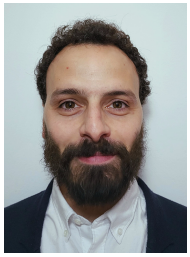

Marco Carlo Rampini, Department of Civil and Environmental Engineering, Politecnico di Milano, Piazza Leonardo da Vinci, 32 - 20133 Milano, Italy. Email: marcocarlo.rampini@polimi.it

Giulio Zani, Department of Civil and Environmental Engineering, Politecnico di Milano, Piazza Leonardo da Vinci, 32 - 20133 Milano, Italy. Email: giulio.zani@polimi.it

Matteo Colombo, Department of Civil and Environmental Engineering, Politecnico di Milano, Piazza Leonardo da Vinci, 32 - 20133 Milano, Italy. Email: matteo.colombo@polimi.it

Marco di Prisco, Department of Civil and Environmental Engineering, Politecnico di Milano, Piazza Leonardo da Vinci, 32 - 20133 Milano, Italy. Email: marco.diprisco@polimi.it

How to cite this article: Flores Ferreira K, Rampini MC, Zani G, Colombo M, di Prisco M. Experimental investigation on the use of Fabric-Reinforced Cementitious Mortars for the retrofitting of reinforced concrete dapped-end beams. Structural Concrete. 2023;24(4):4577–605. https://doi.org/10.1002/suco.202200743